Department of Electronic and Electrical Engineering
University College London

Computations & Simulations for the Design of an Ultra-Sensitive Microwave Cavity

MEng Project
Final Report

Ashlesha Bhagwat
Nikita Malik
Sachi Vaz

Supervisor: Dr Hidekazu Kurebayashi
Second Assessor: Dr Jeroen Elzerman

April 2017

DECLARATION

We have read and understood the College and Department's statements and guidelines concerning plagiarism.

We declare that all material described in this report is substantially our own work except where explicitly and individually indicated in the text. This includes ideas described in the text, figures and computer programs.

Name: …… Signature: ……

Name: …… Signature: ……

Name: …… Signature: ……

Date: ……

Work Breakdown

Section Name	Page No.	Person Responsible
Abstract	1	Nikita Malik
Introduction	6	Nikita Malik
Theory	7	Nikita Malik
Cavity Design	12	Ashlesha Bhagwat
Calculations	18	Sachi Vaz
Characterising existing Cavities	26	Ashlesha Bhagwat
Cu- Al Comparison	38	Sachi Vaz
Simulation Results and Analysis	42	Sachi Vaz
Conclusion	44	Ashlesha Bhagwat
Reflection and Further Work	45 and 47	Nikita Malik

Abstract

The ultimate aim of this project was to design and produce an optimal microwave cavity, in order to facilitate accurate detections of spin dynamics in thin-film samples. Ideally, the resultant cavity needed to have a resonant frequency 2 – 8 GHz and it should also have a high Q-factor.

The project involved characterising existing microwave cavity resonators through a series of lab experiments. The findings from these experiments were used to determine the design of the new cavity with the desired properties. Post production, this cavity will be used to conduct further experiments to measure its effectiveness using FMR and Electric-field-induced FMR.

The initial stage was the most critical; elements such as coupling modes, dimensionality and dielectric materials were investigated to understand their impact on Q-factor and resonant frequency. The two existing cavities were used during these experiments. When deciding on the properties of our final design, material, shape, resonant mode, dielectric material and dimensions were all taken into consideration. Through experiments conducted on these cavities, it was determined that though Aluminium was the cheaper option, Copper yielded more desirable results, hence it was chosen as the material for the final design. After examining the different cavity shape options, cylinder was chosen as it was yielding the lowest resonant frequency. There was a trade-off involved in selecting which mode to couple this cavity to, however, the priority was to achieve a high Q-factor. By trialling a range of dimensions using different dielectrics and their effect on the Q-factor and resonant frequency, three designs were shortlisted which then went through software simulations. Air was chosen as the desirable dielectric and this cavity was operating at resonant mode $TM_{010.}$

TABLE OF CONTENTS

1 Introduction

Spin refers to the intrinsic angular momentum of an electron and Spintronics is the exploitation of this property for various applications. Ferromagnetism, a mechanism by which materials are magnetised, is a direct result of this property.

Electron spin is an electron's intrinsic angular momentum. The spin of any particle is denoted by S. The application of an external magnetic field to a ferromagnetic material causes the dynamic motion of spins. If this spin direction is not the same as the magnetic field, the magnetic energy will be raised from ground-state and eventually, precession will run-down. The relaxation time of magnetic precession is generally less than 1ns.

Ferromagnetic resonance (FMR) is a tool that can be used to probe the spins of ferromagnetic materials. Application of an external magnetic field causes the spins within a sample to align in the direction of the field. This field is driven by microwaves, which cause the spins to precess. Note that for precession to occur, all spins must be excited simultaneously and the direction of the applied microwaves will affect the likelihood of precession occurring. As this precession cannot continue forever, the excess energy is returned as a microwave, illustrating the size of magnetism per unit volume and the precession angle.

A cavity resonator, as designed during this project, is a closed metal structure confining electromagnetic waves within the microwave region. These are also hollow in the middle; this section is used to place a sample for testing purposes. If electromagnetic energy is existent in the cavity, it will bounce off the walls of the cavity and produce standing waves, hence it is classified as a cavity resonator. At frequencies corresponding to the resonant frequency, these waves will produce high field strengths as well as some nulls.

In this report, the phenomena of ferromagnetism and FMR are discussed and utilised to design a highly sensitive microwave cavity resonator.

1.1 Goals and objectives

1.1.1 Overall aim

The overall aim of this project is to design and develop ultra-highly sensitive microwave cavity resonators for spintronic applications. It must ideally have a high Q-factor and fill factor to yield accurate detection of spins.

This is an ongoing research and there already are existent cavities in the lab that ar currently being used for the purposes of this research. The overall goal is to test these cavities and upgrade one using a new design. The current designs will be used as the basis and improvements will be made. In particular, a high quality-factor and also a high filling factor for the final cavity must be achieved as part of this upgrade.

1.1.2 Breakdown of goals:

The following is a list of aims that were realised through the course of the year, from the initial research stage to final simulation and production.

I. Conduct background research into various factors that affect spin detection and how to improve these. Important factors to consider during this research include Q-factor, resonant frequency, different modes that cavity operates in etc.

II. Using research and theory, design an optimal cavity for spin detections with a high Q-factor (in the thousands) and low resonant frequency (between 2 - 8 GHz), whilst taking into account design constraints
III. Characterise current Aluminium and Copper cavities to compare their performance characteristics. This involves the characterisation of sample Q-factor, resonant frequency and other parameters using microwave generator and other MW components
IV. Design improved cavities based on the examined characteristics and simulate them to test against the hypothesis and compare results achieved with the calculated values
V. Produce the final cavity and compare its performance to the calculated values and simulation results
VI. Use the cavity to measure spin dynamics i.e. ferromagnetic resonance. The magnetic field resonance of the cavity will be used to sense the power dissipated while processing the spins. Furthermore, efforts will be made to use the electric field resonance to excite and detect "Electric-Field-Induced" Ferromagnetic Resonance (FMR).

1.1.3 Final deliverables

Deliverable	Deadline
Final Report	28th April 17
Oral Presentation	31st May 17

Table 1:Deliverables leftover including this report.

2 Theory

2.1 Spintronics

Spintronics, a portmanteau of "spin" and "electronics," refers to the manipulation of electron spin for exploitation in applications relating to quantum information processing.

Spin is an intrinsic property of an electron, which describes an angular momentum separate to that caused by orbital motion. Electrons possess their own spin, whilst simultaneously orbiting the nucleus of an atom. A good analogy for visualisation, would be the Earth rotating on its own axis as it orbits the Sun.

Spin can be thought of as a vector quantity, consisting of both magnitude and direction. In the case of electrons, it will take on one of two discrete values: ± ½.

The defining equations for spin angular momentum, *S*, of any physical system are as follows:

$$S = \overline{h}\sqrt{s(s+1)} = \frac{h}{4\pi}\sqrt{n(n+2)} = \overline{h}\sqrt{\frac{1}{2}\left(\frac{1}{2}+1\right)} = \frac{\sqrt{3}}{2}\overline{h}$$

Where $\overline{h} = \frac{h}{2\pi}$ and h is Planck's constant.

Like orbital angular momentum, the spin has an associated magnetic moment that can be denoted as:

$$\mu = \frac{\sqrt{3}}{2}\frac{q}{m_e}\overline{h}$$

Creating a spintronic device requires the generation or manipulation of spin-polarised electrons, typically via the application of an external field. The polarisation of any spin dependent property, X, can be written as:

$$P_X = \frac{X_\uparrow - X_\downarrow}{X_\uparrow + X_\downarrow}$$

A pictorial depiction is provided in figure 1 below.

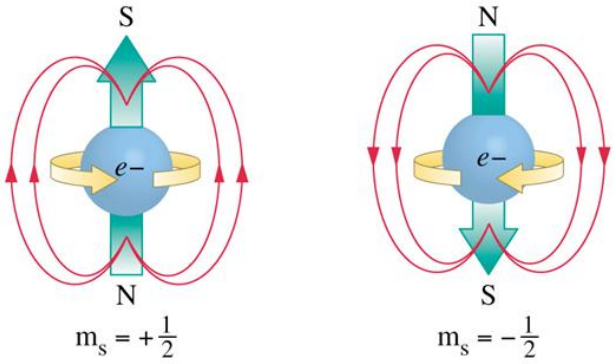

Figure 1: Up and down spins in an electron and corresponding magnetic fields.

2.2 Ferromagnetism

All ferromagnetic materials exhibit a unique ordering phenomenon. This is known as the long-range ordering phenomenon. This means the unpaired electron spins in the ferromagnetic material line up with each other in regions known as domains.

This long rang ordering in ferromagnetic materials is due to the atomic level quantum mechanical interaction. In this interaction, the magnetic moments of the neighbouring atoms are locked in parallel order over a large number of atoms. This is regardless of thermal agitation, which generally causes any atomic level order to randomise. However, not all domains are of the same size. They can range 0.1mm to a couple of mm. The domain itself exhibits strong magnetism. However, overall the material itself is not magnetised, as the domains are orientated randomly in respect to one another. Thus the overall sample is unmagnetised. The diagram below shows pictorially a depiction of a ferromagnetic material, where the electron spins are aligned in each domain. However, the domains themselves are not aligned, leaving the overall sample unmagnetised. (Hyperphysics.com)

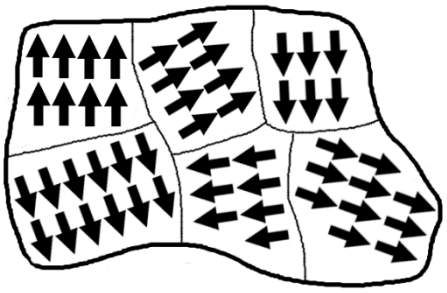

Figure 2: Pictorial depiction of an unmagnetised ferromagnetic material (Wikipedia.org)

The property of Ferromagnetism will be observed when the ferromagnetic material is placed close to a small external magnetic field, like a solenoid. In this situation, the domains will align themselves with each other and the material will be magnetised. This property is depicted in the figure below, where now the domains are all aligned and the overall material is magnet

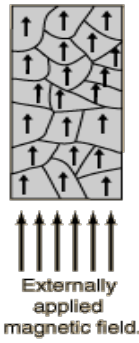

Figure 3: Pictoral depiction of the domain aligning with the external magnetic field. (Hyperphysics.com)

This will cause the external driving magnetic field to be multiplied by a large factor, expressed as the materials relative permeability.

However, it is important to note that more recent evidence in regards to the study of magnetisation shows that the multiplication of the external magnetic field is caused more due to the expansion of the domains already aligned to the external field, rather than the realignment of the domain that are not aligned. This means the domains already aligned with the external field expand at the cost of the not aligned domains shrinking. The diagram below depicts this phenomenon pictorially.

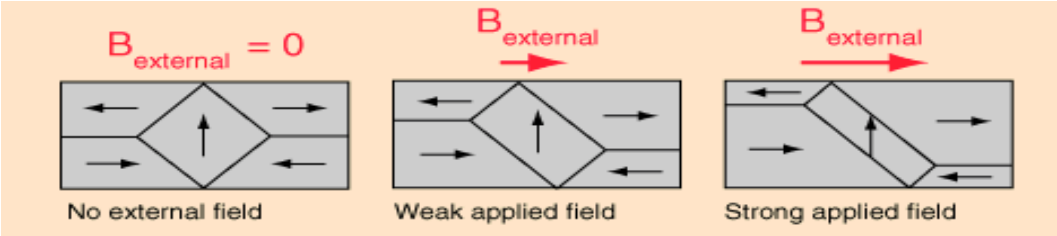

Figure 4: Pictorial depiction of the domain aligning with the external magnetic field at the cost of domains not already aligned. (Hyperphysics.com)

Once the ferromagnetic material is magnetised to saturation, the ferromagnetic material will stay magnetised for a period of time upon the removal of the external field. This property of the ferromagnet to remember its magnetic history is called ‘Hysteresis’. The diagram below shows a typical hysteresis curve.

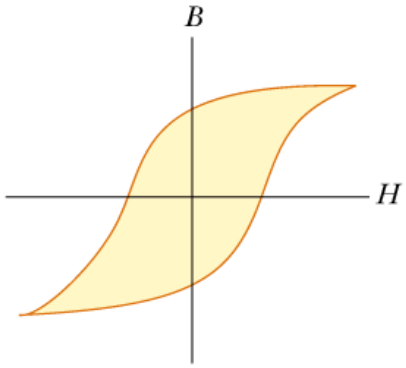

Figure 5: Pictorial depiction of a typical Hysteresis curve (Physik.fu-berlin.de)

The remainder of the saturation magnetisation, left over once the external driving magnetic field is removed is known as remanence of the material. This is an important factor when choosing permanent magnets.

At extremely high temperatures, the ferromagnets lose their ferromagnetic property abruptly due to thermal agitation. This temperature is known as the Curie temperature and is a measure of the energy it takes to actually break the long rage order in Ferromagnetic materials. (Hyperphysics.com)

2.3 Ferro-magnetic resonance (FMR)

FMR is a technique that measures the magnetic properties by detecting the precessional magnetization motion in a ferromagnetic sample.

This happens when the applied external static magnetic fields H_o, causes the magnetic moment to precess around the direction H_{eff}, which is the local field. Then if the sample is radiated with a transverse microwaves, before the relaxation process causes the damping of the precession and the magnetization aligns with H_{eff}. Now if this happens and the microwave frequency corresponds to the precessional frequency then the resonance condition is satisfied and the microwave power is absorbed by the sample.

The magnetisation motion is explained by the Landau-Lifshitz-Gilbert equation, which is shown in the diagram below alongside a pictorial representation of the process.
In the diagram below the part of the equation shaded green represent magnetic moment precession and the yellow part corresponds to the damping caused. (Physik.fu-berlin.de)

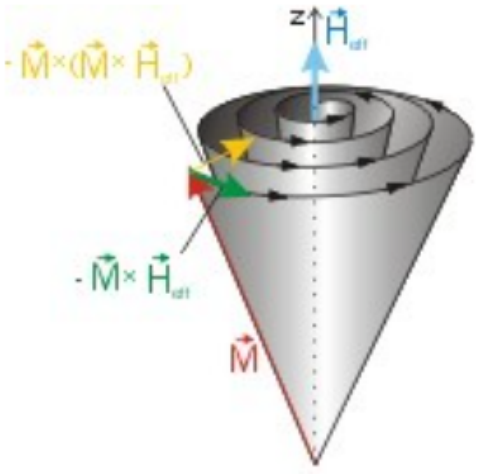

$$\frac{\partial \vec{M}}{\partial t} = -\gamma(\vec{M} \times \vec{H}_{\text{eff}}) + \frac{G}{\gamma M_S^2}\left[\vec{M} \times \frac{\partial \vec{M}}{\partial t}\right]$$

Figure 6: Pictorial depiction of the magnetisation motion (Physik.fu-berlin.de)

On a microscopic level the field H_o causes the Zeeman splitting of the energy levels. The microwave energy is then used to excite microwave dipole transitions between the split energy levels. Thus the energy of the microwaves should correspond to the energy difference of the split-levels. In reality however it is hard to vary the microwave frequency over large ranges thus this is kept constant and the field H_o is varied instead.

This process is shown in the diagram below. The diagram shows the Zeeman splitting and the incoming microwave energy being absorbed at resonance to give a peak.

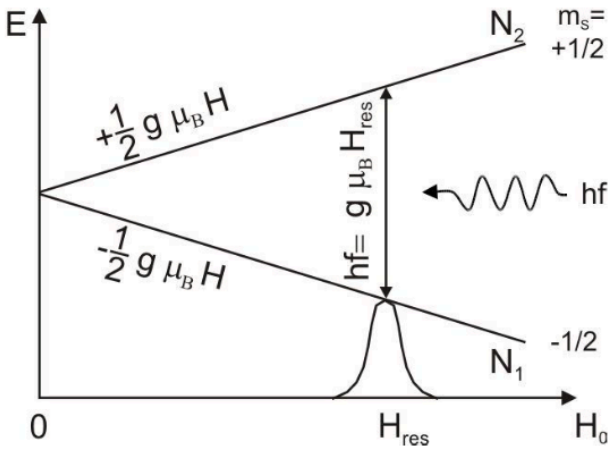

Figure 7: Pictorial depiction of the resonance condition (Physik.fu-berlin.de)

2.4 E-field induced FMR

Using the resonant phenomenon control the spin dynamics means more energy efficient spintronic devices. However, using ferromagnetic resonance excitation to achieve collective spin resonant control requires radio frequency magnetic fields, which is power consuming.
This is where Electric field induced FMR comes in. In this type of FMR, the ferromagnetic resonance is induced directly with an electric field. This considerably reduces the power requirement. This requires however a strong coupling between the electric and magnetic coupling, this itself is difficult to achieve, mainly due to the screening effects of metallic materials.

However, in April 2012, in a paper published in nature magazine, showed an experiment where Electric field induced FMR excitation was demonstrated by using voltage control over the magnetic anisotropy in a few layers of FeCo at room temperature. The technique demonstrated in the research papers provided a low power and highly localised means to control the electron spin dynamics. (Nozaki, T.; Shiota, Y.; Miwa, S.; Murakami, S.; Bonell, F.; Ishibashi, S.; Kubota, H.; Yakushiji, K.; Saruya, T.; Fukushima, A.; Yuasa, S.; Shinjo, T.; Suzuki, Y., 2012). The diagram below is from the research paper in nature, it pictorially shows the concept of Electric-field-induced FMR through voltage control.

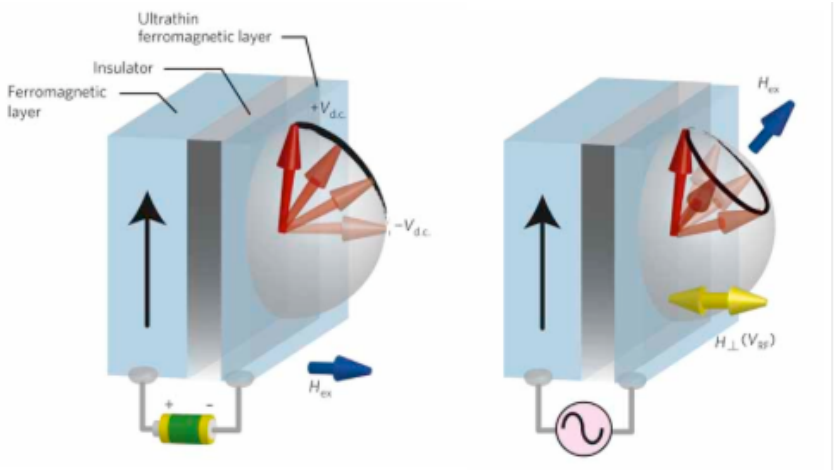

Figure 8: Depiction of the Electric field induced FMR. (Nozaki, T.; Shiota, Y.; Miwa, S.; Murakami, S.; Bonell, F.; Ishibashi, S.; Kubota, H.; Yakushiji, K.; Saruya, T.; Fukushima, A.; Yuasa, S.; Shinjo, T.; Suzuki, Y., 2012)

Diagram on left shows that how the application of a dc voltage can switch the magnetic axis between in-plane and out-of-plane direction. The diagram on right shows how the application of a radiofrequency voltage can excite the FMR dynamics under a static external magnetic field. The yellow arrow is to represent the radiofrequency effective field change.

3 Cavity Design

In this section, we will be discussing the steps taken in designing the final cavity for production. This will include a description of the parameters taken into consideration, such as cavity shape; dielectric material; coupling mode and dimensions. Further to this, any trade-offs and design constraints will be highlighted, along with the overall impact on performance.

Original Cavity: Characterisation

Before launching into our own design, it would be useful to examine the properties of the current cavity and see how they compare to our desired characteristics. These are displayed in the table below.

Shape	Cylinder
Material	Copper (Cu)
Dielectric	PTFE
Resonant Frequency	12 GHz
Q-factor	2,000
Dimensions	a = 9.5 mm, d = 14 mm, t = 3 mm

Table 2: Properties of the original cavity

Conducting a frequency sweep of this cavity, between 11 – 13 GHz, yields the following results.

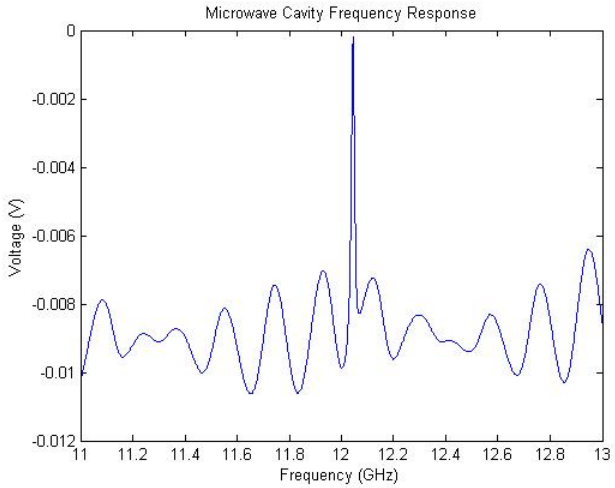

Figure 9: Frequency sweep results for original cavity

A peak can clearly be seen around 12 GHz, which is the resonant frequency. Further analysis of this peak, by calculating the full width at half maximum (FWHM), gives a Q-factor close to 2,000.

3.1 Design Goals

With the final cavity, we hope to achieve two main goals. These are: high Q-factor and low resonant frequency, within the 2 – 8 GHz range.

Having a high Q-factor is important, as it leads to improved sensitivity and signal-to-noise ratio (SNR). Ideally, the microwaves should be absorbed by the sample across a narrow frequency range. This is especially useful, since the purpose of the cavity is to provide more accurate detections of spin dynamics.

Resonant frequency is another critical factor, for the following reasons:

1. Much of the support equipment operates within a given frequency range. This equipment becomes more expensive as the operating frequency increases. Therefore, a lower resonant frequency is preferred due to costs and ease.

2. If the resonant frequency is low, but there is a lot of surrounding noise, the experiment could be done at a multiple of the resonant frequency. However, the higher the resonant frequency, the lesser the number of multiples that can be tried.

3. We need to ensure that, at our chosen resonant frequency, multiple modes are not excited. If another mode (apart from the one we have decided operate at) is active, this might lead to undesirable behaviour.

3.2 Parametric Considerations

In this sub-section, we individually discuss each of the critical parameters in the design of the final cavity. These will be examined with respect to, design constraints; desirable properties and effect on Q-factor and resonant frequency.

Cavity Material

We were presented with two main options of materials, from which the cavity could be constructed. These were aluminium (Al) and copper (Cu). The limited range of materials fit for purpose, is due to restrictions imposed by production, performance and cost. Although an element such as platinum (Pt) would be ideal, this is not practical due to the expense.

One of the primary advantages of Al, is that it is cheaper. In addition, during experimentation, the location of the cavity on the magnet requires it to be lightweight. This is another advantage of using Al. However, one of the drawbacks is that the material oxidises in air. This leads to degradation of Q-factor over time. Moreover, Al retains its sheen, making it difficult to determine when oxidation has occurred.

Cu suffers from similar problems, with regards to degradation of Q-factor. In contrast to Al, it acquires a green hue upon oxidation. This can be prevented by gold-plating the cavity, but we cannot do this because of the aforementioned restrictions.
Despite its drawbacks, Cu is better suited to the purposes of our experiment. It is also a tried-and-tested material. With this in mind, we decided to construct our cavity from Cu.

Shape

In order to determine the best shape to use, we were told to explore cylinders, rectangles and hexagonal cylinders. Later, we further narrowed our options to either a rectangular or cylindrical cavity. Hexagonal cylinders were discarded, due to the lack of sufficient literature available to form a hypothesis.

We first looked at rectangular cavities, as these are easiest to construct. The graph below, shows the excited modes at different resonant frequencies.

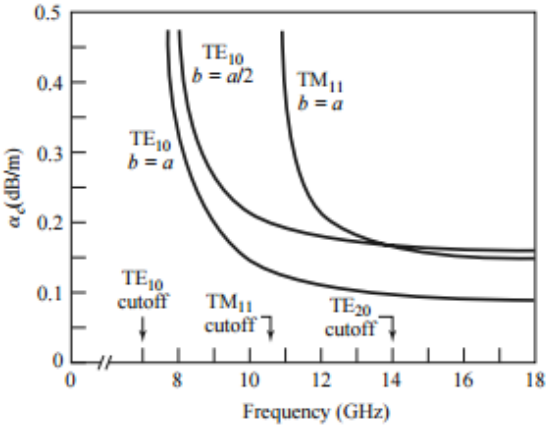

Figure 10: Rectangular cavity modes (Pozar)

It can be seen that the lowest possible resonant frequency, using a rectangular cavity, is 8 GHz. This is not sufficiently low for our purposes. Therefore, we chose to limit our design to solely cylindrical shapes.

3.3 Coupling Modes

In light of the previous findings, we decided to explore the aspects of cylindrical cavities that might yield the desired properties. We began by exploring the choice of TEM modes that can be coupled to and the resulting effect on Q-factor and resonant frequency. It was communicated to us, that a choice of either TM_{010} or TE_{111} is preferred. Therefore, we limit our assessment to these modes.

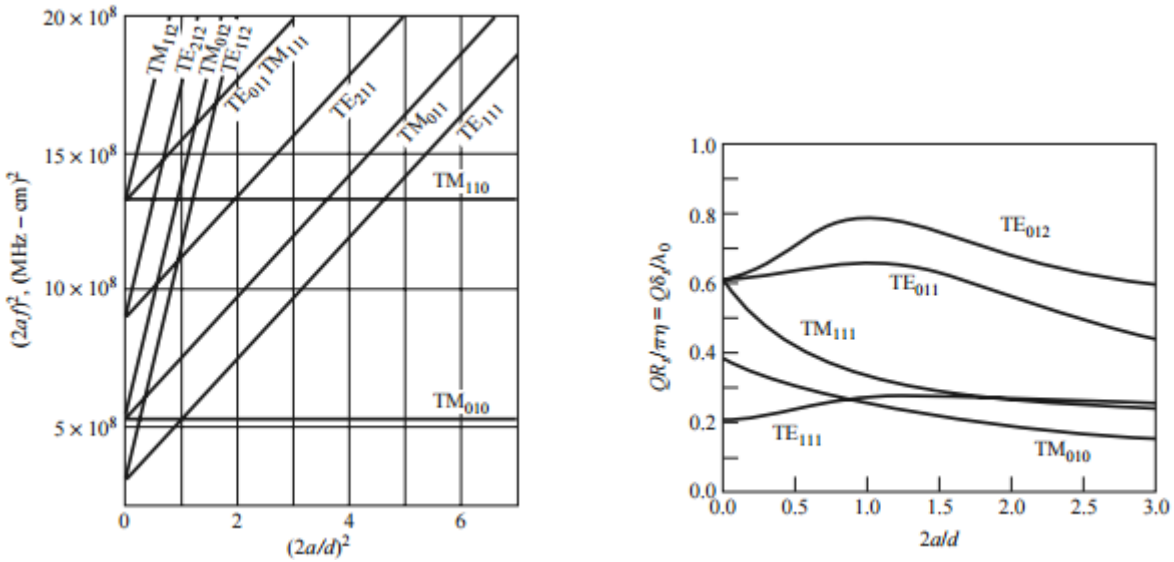

Figure 11: Resonant frequency vs. a/d ratio (Pozar) (left) and Figure 12: Q-factor vs. a/d ratio (Pozar) (right)

There is a clear trade-off involved in selecting which mode to couple to. For TE_{111}, there is a narrow range of a/d ratios for which the resonant frequency is lower than the TM_{010} mode. The advantage of this, is that lower frequencies are more desirable. However, within this limit, the Q-factor is also lower than that of the TM_{010} mode.

We also undertook a series of calculations to determine the range of resonant frequencies obtained for each mode. It was found that a much lower resonant frequency can be obtained in the TM_{010} mode, as opposed to other modes. See Appendices B - D for details.

Other important considerations in deciding which mode to couple to, are the orientation of field lines and coupling wire set-up. The resulting field lines, from coupling to either one of these modes, are displayed below.

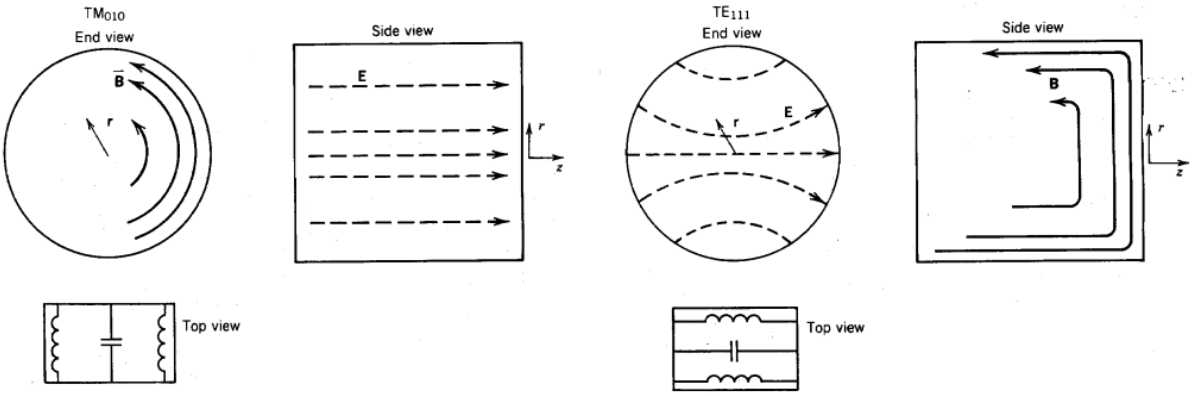

Figure 13: Field lines for different modes (Resonant Cavities and Waveguides, MIT)

It can be observed that, for the TM_{010} mode, the E-field inside the cavity will comprise straight lines. For the TE_{111} mode, the B-field inside the cavity will form concentric rings. Ideally, we want the field lines to be straight. Therefore, TM_{010} is a better choice.
The image below, shows the different ways of coupling to the TM_{010} mode in a cylindrical cavity.

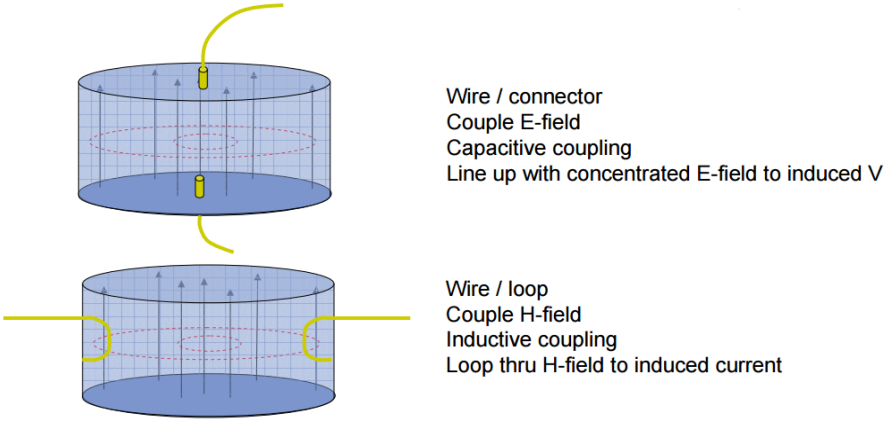

Figure 14: Coupling to TM010 (R. Kwok)

As mentioned earlier, the coupling wire set-up is important to consider. For simplicity of production, we want our coupling wire to be aligned with the cylinder's vertical axis of symmetry. In this way, it should extend from the top flat surface through to the bottom. It is possible to couple to the TM_{010} mode this way, using the configuration in the top image.

As a result of the previous findings, we decided that our final cavity should couple to the TM_{010} mode. To obtain a high Q-factor, it would be useful to have a low a/d ratio. This would manifest in the form of a tall, thin cylinder. The corresponding E-field would consist of straight lines and the wire could go right through the middle from one of the circular end surfaces.

Dielectric

Next, we began exploring various options for the dielectric with the following constraints:

- Easily moulded into a cylindrical shape
- Transparent to electric and magnetic fields

- Electrically insulating but thermally conductive (if possible)

The original cavity contains polytetrafluoroethylene (PTFE). Another material to consider, would be FR4.

FR4 is manufactured from fibreglass cloth embedded in epoxy resin. Its key properties are extremely high mechanical strength; good dielectric loss and electrical strength. FR4 has a relative permittivity of 4.5, which is slightly dependent on frequency. This is higher than PTFE's relative permittivity of 2.1, demonstrating that FR4 is more transparent to electric fields.
Additionally, the relative permeability of FR4 is 1, whereas, the relative permeability of PTFE is many orders of magnitude smaller. Therefore, PTFE is more transparent to magnetic fields than FR4.

Comparing loss tangents at 3 GHz (within our target resonant frequency range), FR4 has a value of 0.018. This is higher than that of PTFE, which is 0.0015. FR4 also has a dielectric thermal in-plane and through-plane conductivity of 0.81W/mK and 0.29W/mK respectively.
With regards to ease of moulding, PTFE is more malleable than FR4. Both the materials are electrically insulating and have a thermal conductivity of approximately 0.25W/mK.
As both materials satisfy the requirements listed above, we decided to perform calculations with each of them. The resulting Q-factor and resonant frequency values, would then be used as a basis to determine which material to incorporate in our final design.

Calculations

This sub-section outlines the steps taken to calculate the Q-factor and resonant frequency for our cavity. The variables in our calculations are dielectric material and cavity dimensions. We considered Air, PTFE and FR4.
The cavity wall thickness must exceed 2 mm, for production. In addition, it would be ideal for the cylinder radius to be between 6 – 8 mm and the length to be between 10 – 80 mm.

3.4 Resonant Frequency

In order to calculate the resonant frequency, for a given dielectric and set of dimensions, we used the following equation (Pozar).

$$f_{nml} = \frac{c}{2\pi\sqrt{\mu_r \varepsilon_r}} \sqrt{\left(\frac{p_{nm}}{a}\right)^2 + \left(\frac{l\pi}{d}\right)^2}$$

The value of p_{nm} is independent of dimensions or the dielectric and, instead, depends on the mode being excited. For TM_{010}, it has a value of 2.405.
In this equation, a represents the radius and d represents the length of the cavity. For our calculations, we kept the a/d ratio constant at a value of 0.5, as this is the standard used in cavity design and avoids unnecessary complexity.

Our first set of calculations assumes air to be the dielectric. Therefore, we only had to vary a to observe the effect on resonant frequency. In doing this, we discovered a trade-off. In order to achieve a low resonant frequency, we require a relatively high value for a. However, this is in conflict with our requirement to keep a within the 6 – 8 mm range. As we found out, for air, the lowest value of a resulting in a resonant frequency below 8 GHz is 14.5 mm.
The same process outlined above was then repeated for PTFE and FR4 dielectrics. The results are summarised in the table below.

Dielectric	min{*a*} < 8 GHz (mm)	*d* (mm)
Air	14.5	29
PTFE	10	20
FR4	6.8	13.6

Table 3: Minimum radius to match resonant frequency requirements for a given dielectric

3.5 Q-Factor

In order to calculate Q-factor, we used the following equation (Microwave Engineering, D.M. Pozar).

$$Q_0 = \left(\frac{1}{Q_c} + \frac{1}{Q_d}\right)^{-1}$$

In determining the Q-factor for the cavity, we calculated its value using two different equations. The first (below – left), is from the book cited above. The second (below – right) is from a text published by the University of Gävle, the link for which is provided in the references below.

$$Q_c = \frac{ka\eta}{2R_s} \qquad\qquad Q_c = \frac{2V}{S\sqrt{\frac{2}{\omega\mu\sigma}}}$$

We took σ to be approximately 5.81×10^7 S/m. This is the conductivity of copper and remains constant in our calculations. The angular frequency, ω, can simply be calculated by multiplying the resonant frequency (shown earlier) by 2π. V and S represent the cylinder volume and surface area, respectively. When calculating these, we assumed a solid and closed cylinder. We also used the following equations (Microwave Engineering, D.M. Pozar), in intermediate calculations.

$$R_s = \sqrt{\frac{\omega\mu}{2\sigma}} \qquad\qquad \eta = \sqrt{\frac{\mu}{\varepsilon}}$$

Although the resulting values for Q-factor different slightly (depending on Q_c equation used), the order of magnitude remained the same. Therefore, we averaged the two values to get our final result. Using the same dimensions as above, which keep us within the desired resonant frequency range, the overall results are as follows.

Material	Dielectric	a (mm)	d (mm)	f (GHz)	Q-factor
Copper	Air	14.5	29	7.9	16,000
Copper	PTFE	10	20	7.9	630
Copper	FR4	6.8	13.6	7.9	62

Table 4: Resonant frequency and Q-factor for different dielectrics

As shown by the table above, FR4 results in a much lower Q-factor than the other two. This is because it has a much larger loss tangent, resulting in a higher value for the dielectric Q-factor, Q_d. Therefore, this value dominates in the equation and the overall Q-factor (Q_0) remains small. Hence, we discard FR4 as a potential option.

Of the remaining two, air provides a much higher Q-factor. It is important to note, that the calculated Q-factor is very high because the theoretical equations assume perfect conditions. Obviously, this will not be the case in the laboratory and so the experimental value is expected

to be lower. Losses will typically be a percentage of the theoretical Q-factor. As a result, it is better to have a high theoretical value.
For the reasons outlined above, we decided to have air as the dielectric in our final cavity.

3.6 Final Design and Simulations

In order to test our hypothesis, we decided to run some simulations. The model used was for a cylindrical copper cavity, coupled to the TM_{010} mode, with air as the dielectric and a radius of 14.5 mm.

One point, briefly mentioned earlier, is that the two cavity Q-factor equations result in slightly different values. The first one (left), is only valid if the a/d ratio is kept at 0.5. In contrast, the second one (right) does not have this restriction. Therefore, we ran some further calculations to test the effect of changing the cavity length (d) on Q-factor, whilst keeping a constant.
We found that a higher value of d, yields a higher Q-factor without affecting the resonant frequency (See Appendix A). This is likely due to the increased volume and surface area. Conversely, a smaller d may lead to improved sensitivity due to the increased ratio of sample size to cavity volume. Hence, there is a trade-off.

In our simulations, we wanted to test if altering the cavity length affects the Q-factor, as predicted. The dimensions simulated, along with theoretical results, are presented below.

a (mm)	d (mm)	f (GHz)	Q-factor
14.5	50	7.9	15,300
14.5	29	7.9	13,160
14.5	10	7.9	8,000

Table 5: Simulation dimensions with predicted Q-factor and resonant frequency

It is worth noting that the Q-factors calculated above are a little different to those displayed earlier, for air. This is because those Q-factors were based on an average of the values calculated from the two equations. Those in table 4, are only calculated using the second equation.

4 Calculations

As described in the Cavity Design (section 3) we decided on a cylindrical cavity for our final design. Further, we performed calculation with 3 dielectric materials PTFE, Air and FR4. We performed the calculations for a copper cavity, as this was our material of choice, the reasoning for which was described in the Comparison between Cu and Al (section 5). The formulas used for the calculations are given below and are summarised with the other factors in the Cavity Design (section 3). It is also important to note that all calculations were performed for the TM010 mode, the reasoning for which is provided in the Cavity Design (section 3).

4.1 Methods used for calculating Q factors:

As mentioned in the Cavity designed (section 3) of the report we used 2 formulas to calculate Q factor. Both the formulas are described in more detail in this sub-section.

The first method (**method 1**) used to calculate Q factor is mentioned by the set of equations detailed below. It should be noted that the below equations apply when coupling to TM modes only.

The procedure for the complete calculation is as follows:

a) Calculate the resonant frequency, f_{nml} where nml stands for the TM mode number 010 respectively in this case. The formulae for this is:

$$f_{nml} = \frac{c}{2\pi\sqrt{\varepsilon_r \mu_r}} \sqrt{\left(\left[\frac{l\pi}{d}\right]^2 + \left[\frac{p_{nm}}{a}\right]\right)^2}$$

where, a is the radius, d is the length and P_{nm} is a constant.
The constant value for P_{nm} for the TM010 mode is 2.405, which we used. The values of Pnm for TM modes of circular waveguides are shown in the table below:

n	P_{n1}	P_{n2}	P_{n3}
0	2.405	5.520	8.654
1	3.832	7.016	10.174
2	5.135	8.417	11.620

Figure 15: Table showing the Pnm constants

b) Then using the value of f_{nml} obtained in step 1, we calculate K, which is the wavenumber of the resonant cavity.

$$k = \frac{2\pi f_{nml}\sqrt{\varepsilon_r}}{c}$$

c) The next step is to calculate the value of R_s again using the frequency obtained in step 1.

$$R_S = \sqrt{\frac{\omega\mu}{2\sigma}}$$

d) Then the value of η is calculated using

$$\eta = \sqrt{\frac{\mu}{\varepsilon}}$$

e) Then we calculate Q_c, which is the Q factor of the cylinder.

$$Q_C = \frac{Ka\eta}{2R_S}$$

f) The next step is calculating Q_d, which is the Quality factor of the dielectric material used inside the cavity.

$$Q_d = \frac{1}{tanD}$$

Where tanD is the dielectric loss and it varies with frequency. For the purposes of our experiments we need the value of tanD at 3GHz. We used tanD at 3GHz as it falls within our target resonant frequency range of 2-8GHz.

g) Finally, using the values of Q_c and Q_d we can calculate the normalised Q factor Q_o, due to losses from various conducting modes.

$$Q_O = \left(\frac{1}{Q_C} + \frac{1}{Q_d}\right)^{-1}$$

It is important to note here that in the Q factor calculations using the method above, we kept d = 2*a, as the equations described above to calculate Q factor is only valid under this condition. It is also important to note that due to this the a/d ratio is always 0.5. Thus, in the comparison graphs, we decided to analyse the effect of changing the radius (a) on the resonant frequency and Q factor, rather than the effect of the a/d ratio as this always remains at 0.5.

The second method (**method 2**) used for calculating Q_C is mentioned below. This was used to get values for Q_2, using the same method to obtain Q_d and Q_o as mentioned in steps f) and g) above:

$$Q_C = \frac{2V}{S\sqrt{\frac{2}{\omega\mu\sigma}}}$$

where S and V are the volume and surface area of the cavity resonator respectively. σ is the conductivity of the metal wall.

As mentioned in the Cavity design section the Q factors obtained from both these Q factor equations are averaged to obtain a final single Q factor value.

4.2 Calculations for Air:

4.2.1 Table summarising the constant values used for Air:

Air	
Relative Permeability	1
Relative Permittivity	1.000536
P_{nm} (P_{01} for TM010)	2.405
Vacuum permeability	0.00000125
Conductivity Copper	59600000
μ_0	0.00000125
e_0	8.854E-12
$\eta=\sqrt{(\mu/e)}$	375.633
tanD 3GHz	0

Table 6: Table of the constant values used for Air calculations

4.2.2 Obtained table of results for Air:

Using the 2 Q factor calculation methods described in the above section, we obtain the following table of results. Q_{c1} is the obtained Q factor using method 1 and Q_{c2} is the obtained Q factor using method 2 described above.

a(m)	d(m)	a/d	Fnml (Hz)	K	Rs	η	S (m^2)	V (m^3)	Q_{01}	Q_{02}	Average Q
0.0045	0.009	0.5	25,511,028,057	533.401	0.0410	375.63	0.00038	5.726E-07	10995.86	7330.58	9163.22
0.0055	0.011	0.5	20,872,659,319	436.419	0.0371	375.63	0.00057	1.045E-06	12156.39	8104.26	10130.32
0.0065	0.013	0.5	17,661,480,962	369.277	0.0341	375.63	0.00080	1.726E-06	13215.38	8810.26	11012.82
0.0075	0.015	0.5	15,306,616,834	320.040	0.0318	375.63	0.00106	2.651E-06	14195.60	9463.73	11829.67
0.0085	0.017	0.5	13,505,838,383	282.389	0.0298	375.63	0.00136	3.859E-06	15112.37	10074.91	12593.64
0.0095	0.019	0.5	12,084,171,185	252.663	0.0282	375.63	0.00170	5.387E-06	15976.62	10651.08	13313.85
0.0105	0.021	0.5	10,933,297,739	228.600	0.0268	375.63	0.00208	7.274E-06	16796.46	11197.64	13997.05
0.0115	0.023	0.5	9,982,576,196	208.722	0.0256	375.63	0.00249	9.556E-06	17578.10	11718.74	14648.42
0.0125	0.025	0.5	9,183,970,100	192.024	0.0246	375.63	0.00295	1.227E-05	18326.44	12217.63	15272.03
0.0135	0.027	0.5	8,503,676,019	177.800	0.0237	375.63	0.00344	1.546E-05	19045.40	12696.93	15871.16
0.0145	0.029	0.5	7,917,215,604	165.538	0.0228	375.63	0.00396	1.916E-05	19738.18	13158.79	16448.48
0.0155	0.031	0.5	7,406,427,500	154.858	0.0221	375.63	0.00453	2.340E-05	20407.46	13604.97	17006.22

Table 7: Table of results obtained for Air calculations

**Note that Q_d for air is 0, thus is not included as another column in the above table.*

4.2.3 Relationship Graphs for Air:

The purpose of the graphs below is to demonstrate how the Q factor and resonant frequency vary with the cavity dimensions.

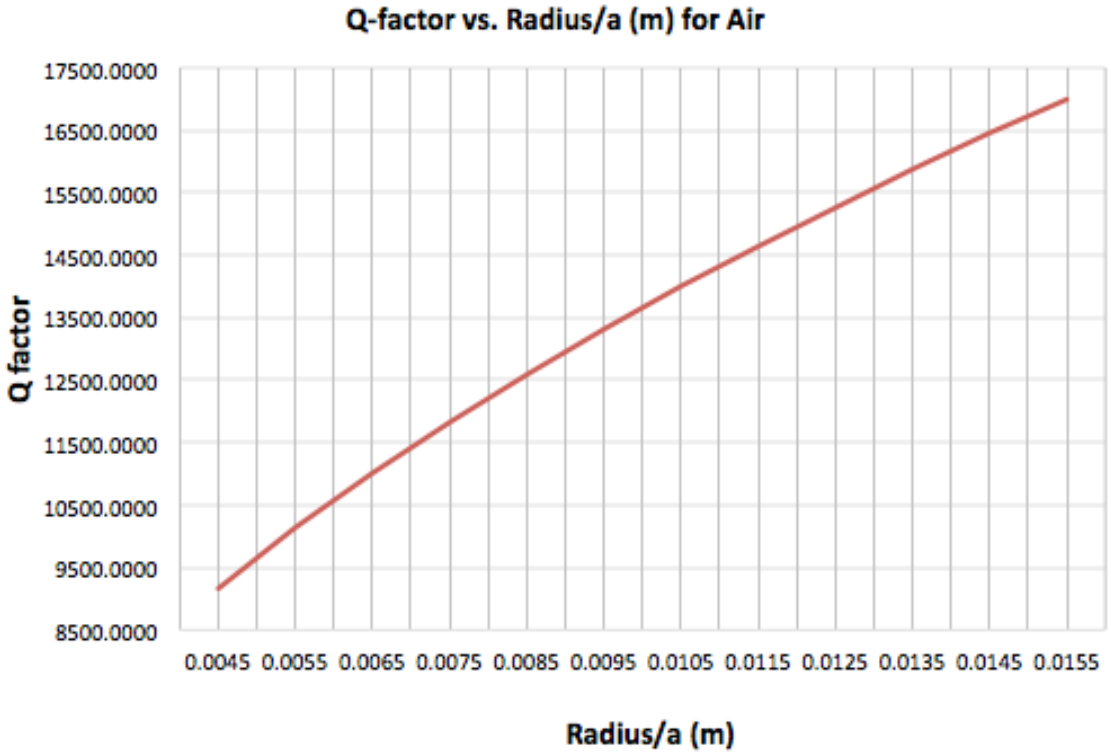

Figure 16: Q-factor vs Radius for Air

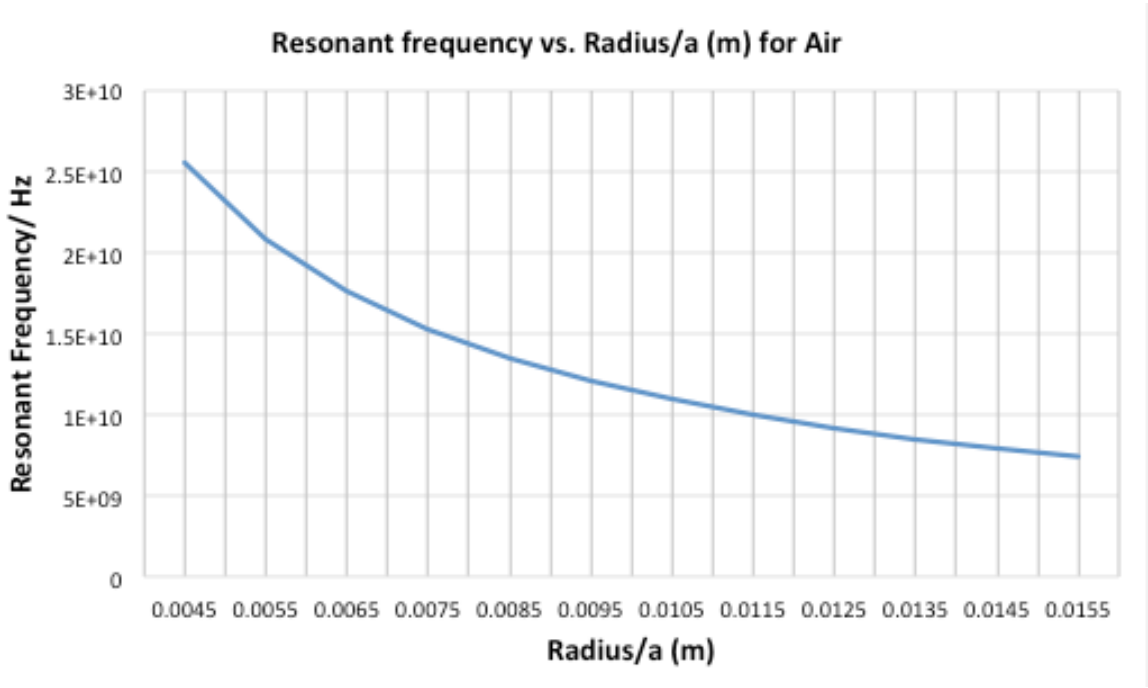

Figure 17: Resonant Frequency vs Radius for Air

4.2.4 Analysis

From the calculations and the plotted graphs, it can be seen that the Q factor keeps increasing as the radius of the cavity increases. On the other hand, the resonant frequency decreases as the radius increases. Thus, if we were to choose air as a dielectric we need to find a spot on these 2 graphs that satisfy our previously mentioned design requirements (resonant frequency between 6-8GHz and Q factor as high as possible, alongside an ideal radius of 10mm). Thus, from looking at the table of results for air, we believed that the radius size of 14.5mm that has a 7.9 GHz resonant frequency and gives a Q factor of approximately 16000 would best suit our needs. This is highlighted and summarised in the Cavity Design (section 3) of our report.

4.3 Calculations for FR4:

4.3.1 Table summarising the constant values used for FR4:

FR4	
Relative Permeability	1
Relative Permittivity	4.5
P_{nm} (P_{01} for TM010)	2.405
Vacuum permeability	0.00000125
Conductivity Copper	59600000
μ_0	0.00000125
e_0	8.8542E-12
$\eta=\sqrt{(\mu/e)}$	177.1226
tanD 3GHz	0.016

Table 8: Table of the constant values used for FR4 calculations

4.3.2 Obtained table of results for FR4:

Using the 2 Q factor calculation methods described in the above section, we obtain the following table of results. Q_{c1} is the obtained Q factor using method 1 and Q_{c2} is the obtained Q factor using method 2 described above.

a(m)	d(m)	a/d	Fnml (Hz)	K	Rs	η	S (m^2)	V (m^3)	Q_d	Q_{01}	Q_{02}	Average Q
0.0045	0.009	0.5	12029236496	533.401	0.0282	177.12	0.000382	5.73E-07	62.5	61.99	61.73	61.86
0.0055	0.011	0.5	9842102588	436.419	0.0255	177.12	0.00057	1.05E-06	62.5	62.04	61.81	61.92
0.0065	0.013	0.5	8327932959	369.277	0.0234	177.12	0.000796	1.73E-06	62.5	62.07	61.86	61.97
0.0068	0.0136	0.5	7960524152	352.986	0.0229	177.12	0.000872	1.98E-06	62.5	62.08	61.88	61.98
0.0075	0.015	0.5	7217541898	320.040	0.0218	177.12	0.00106	2.65E-06	62.5	62.10	61.90	62.00
0.0085	0.017	0.5	6368419321	282.389	0.0205	177.12	0.001362	3.86E-06	62.5	62.13	61.94	62.03
0.0095	0.019	0.5	5698059393	252.663	0.0194	177.12	0.001701	5.39E-06	62.5	62.15	61.97	62.06
0.0105	0.021	0.5	5155387070	228.600	0.0184	177.12	0.002078	7.27E-06	62.5	62.16	62.00	62.08
0.0115	0.023	0.5	4707092542	208.722	0.0176	177.12	0.002493	9.56E-06	62.5	62.18	62.02	62.10
0.0125	0.025	0.5	4330525139	192.024	0.0169	177.12	0.002945	1.23E-05	62.5	62.19	62.04	62.11
0.0135	0.027	0.5	4009745499	177.800	0.0163	177.12	0.003435	1.55E-05	62.5	62.20	62.06	62.13

Table 9: Table of results obtained for FR4 calculations

4.3.3 Relationship Graphs for FR4

The purpose of the graphs below is to demonstrate how the Q factor and resonant frequency vary with the cavity dimensions.

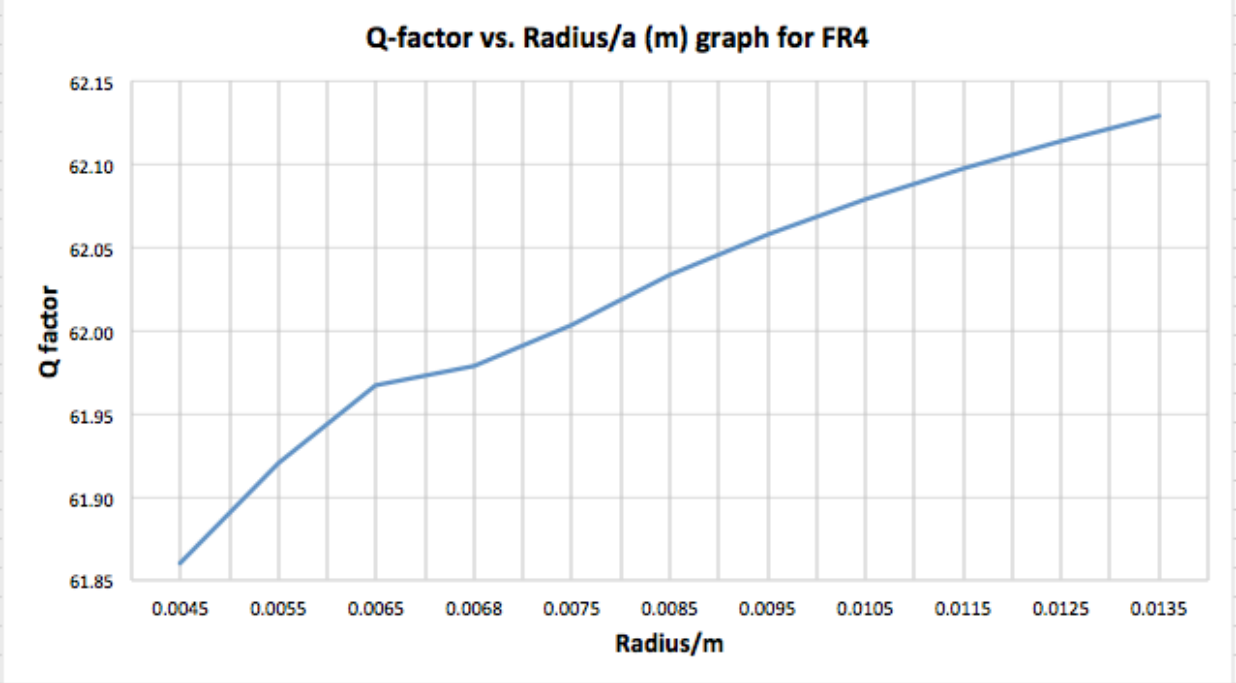

Figure 18: Q-factor vs Radius for FR4

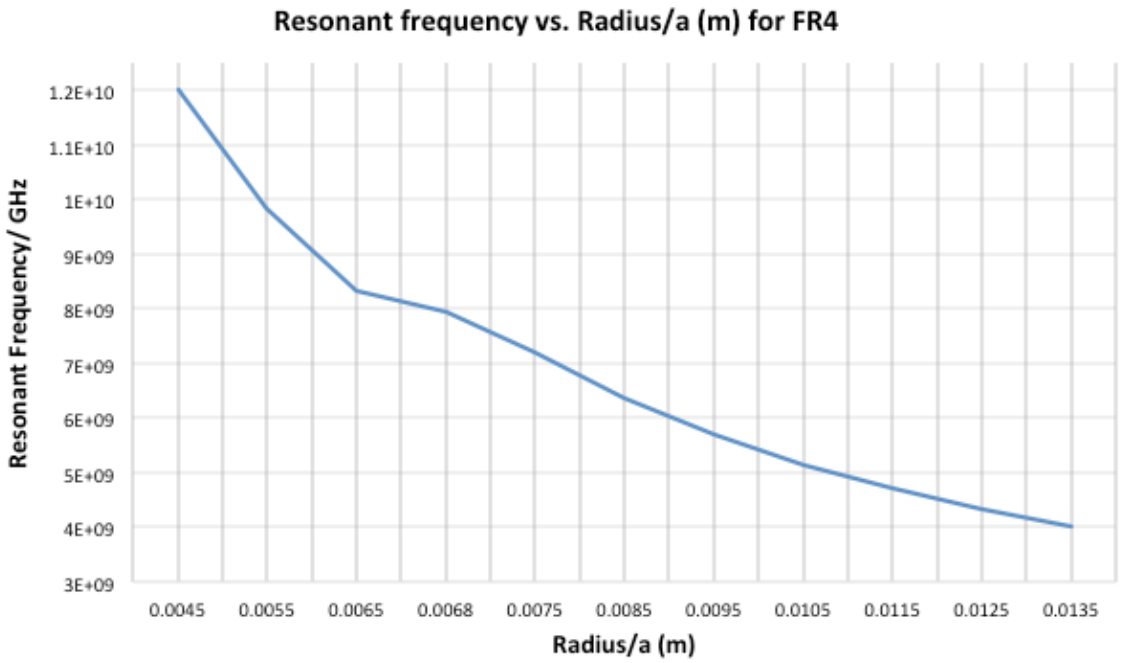

Figure 19: Resonant Frequency vs Radius for FR4

4.3.4 Analysis

From the calculations and the plotted graphs it can be seen that the Q factor keeps increasing as the radius of the cavity increases. On the other hand the resonant frequency decreases as the radius increases. This is a similar trend to what was observed with Air as a dielectric. Thus, if we were to choose FR4 as a dielectric we need to find a spot on these 2 graphs that satisfy our previously mentioned design requirements (resonant frequency between 6-8GHz and Q factor as high as possible, alongside an ideal radius of 10mm). After looking at the table of results for FR4, we added another row of radius 0.0068m; this gave us a resonant frequency within the desired range and a Q factor of 62.

4.4 Calculations for PTFE

4.4.1 Table summarising the constant values used for PTFE

PTFE	
Relative Permeability	1
Relative Permittivity	2.1
P_{nm} (P_{01} for TM010)	2.405
Vacuum permeability	0.00000125
Conductivity Copper	59600000
μ_0	0.00000125
e_0	8.8542E-12
$\eta=\sqrt{(\mu/e)}$	259.281
tanD 3GHz	0.0015

Table 10: Table of the constant values used for PTFE calculations

4.4.2 Obtained table of results for PTFE:

Using the 2 Q factor calculation methods described in the above section, we obtain the following table of results. Q_{c1} is the obtained Q factor using method 1 and Q_{c2} is the obtained Q factor using method 2 described above.

a(m)	d(m)	a/d	Fnml (Hz)	K	Rs	η	S (m^2)	V (m^3)	Q_d	Q_{01}	Q_{02}	Average Q
0.0045	0.009	0.5	17608999161	533.401	0.0341	259.3	0.00038	5.73E-07	666.67	621.33	600.89	611.11
0.0055	0.011	0.5	14407362950	436.419	0.0308	259.3	0.00057	1.05E-06	666.67	625.39	606.60	616.00
0.0065	0.013	0.5	12190845573	369.277	0.0283	259.3	0.00080	1.73E-06	666.67	628.50	611.02	619.76
0.0075	0.015	0.5	10565399497	320.040	0.0264	259.3	0.00106	2.65E-06	666.67	631.00	614.56	622.78
0.0085	0.017	0.5	9322411320	282.389	0.0248	259.3	0.00136	3.86E-06	666.67	633.05	617.49	625.27
0.0095	0.019	0.5	8341104866	252.663	0.0234	259.3	0.00170	5.39E-06	666.67	634.78	619.96	627.37
0.0100	0.020	0.5	7924049622	240.030	0.0228	259.3	0.00188	6.28E-06	666.67	635.55	621.06	628.31
0.0105	0.021	0.5	7546713926	228.600	0.0223	259.3	0.00208	7.27E-06	666.67	636.27	622.09	629.18
0.0115	0.023	0.5	6890477933	208.722	0.0213	259.3	0.00249	9.56E-06	666.67	637.56	623.94	630.75
0.0125	0.025	0.5	6339239698	192.024	0.0204	259.3	0.00295	1.23E-05	666.67	638.70	625.58	632.14
0.0135	0.027	0.5	5869666387	177.800	0.0197	259.3	0.00344	1.55E-05	666.67	639.71	627.04	633.38

Table 11: Table of results obtained for PTFE calculations

4.4.3 Relationship Graphs for PTFE

The purpose of the graphs below is to demonstrate how the Q factor and resonant frequency vary with the cavity dimensions.

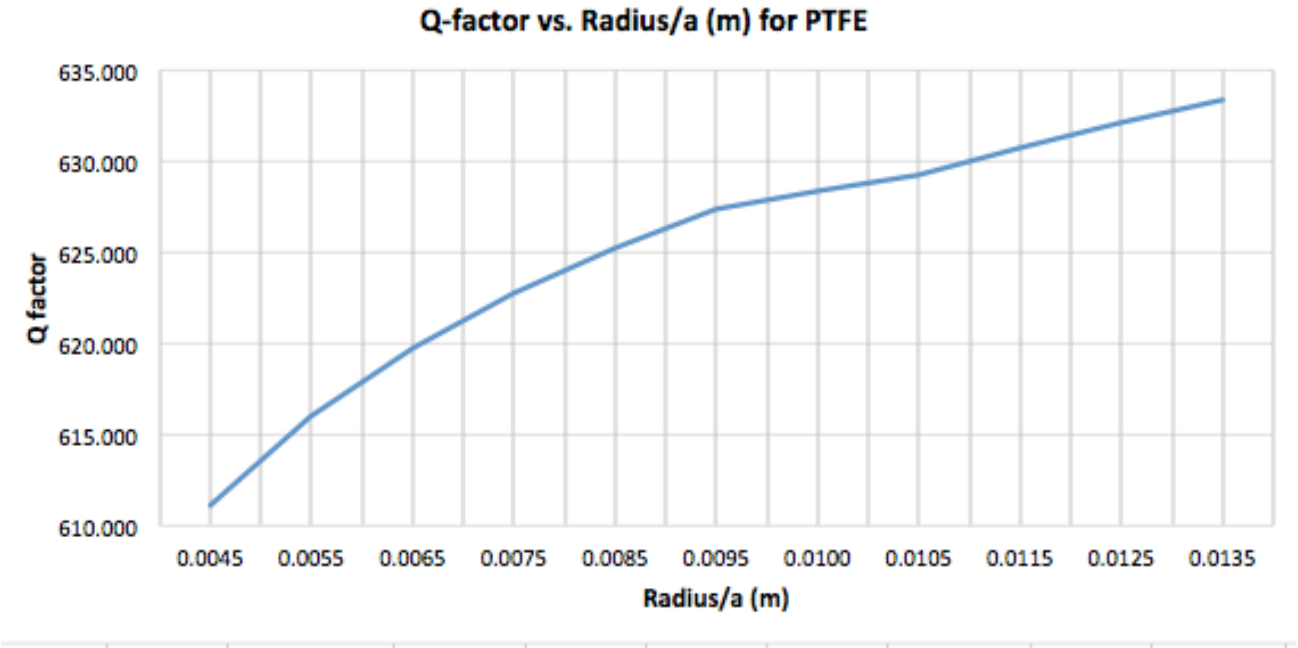

Figure 20: Q-factor vs Radius for PTFE

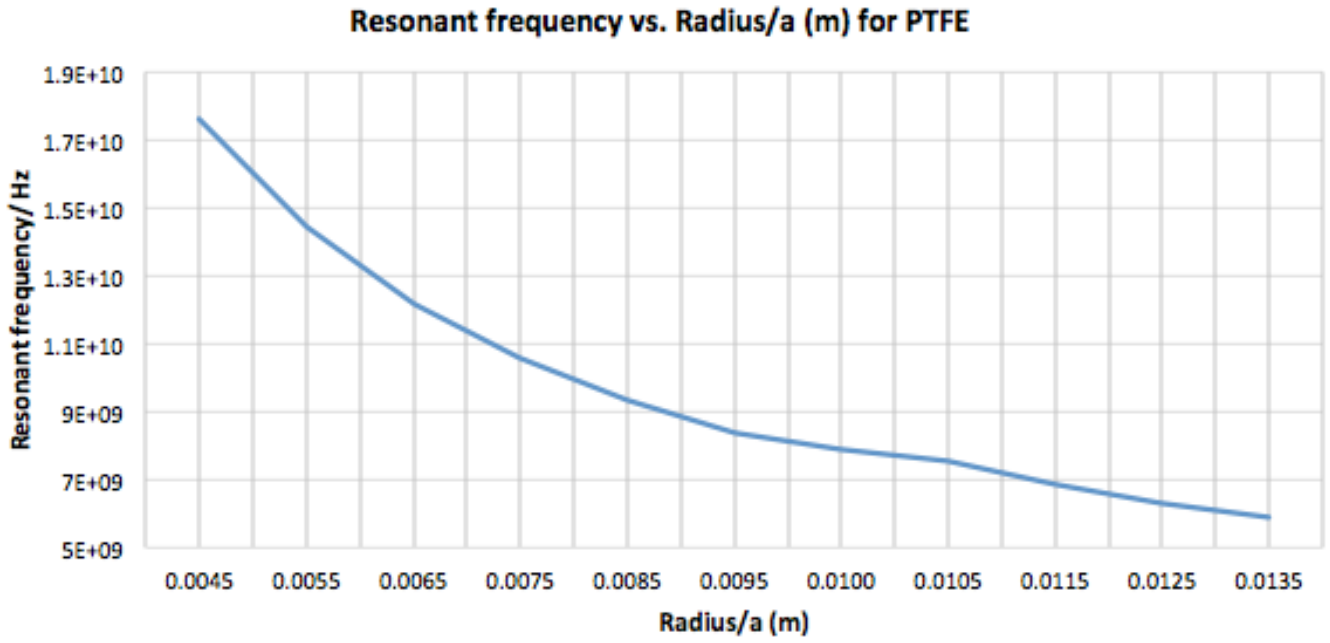

Figure 21: Resonant Frequency vs Radius for PTFE

4.4.4 Analysis

From the calculations and the plotted graphs, it can be seen that the Q factor and the resonant frequency follow a similar trend to that seen in FR4 and Air. Thus, if we were to choose PTFE as a dielectric we need to find a spot on these 2 graphs that satisfy our previously mentioned design requirements (resonant frequency between 6-8GHz and Q factor as high as possible, alongside an ideal radius of 10mm). After looking at the table of results for PTFE, we added another row of radius 0.0010m; this gave us a resonant frequency within the desired range of 7.9GHz and a Q factor of 628.

A summary of the final dimensions chosen for each of the 3 dielectric materials is provided in the Cavity Design (Section 3) of the report.

4.5 Calculations Conclusion

From this section we can conclude that it is possible to redesign the cavity to match our requirements mainly having a high Q factor and a resonant frequency between 2-8GHz.

5 Characterising Cavities

In order to validate our hypothesis for the new cavity design (see Work-Plan 1), we will need to characterise it in a controlled laboratory environment through conducting a series of experiments. However, before proceeding, it would be useful to characterise the two original cavities (Al and Cu). The purpose of this, is to set some performance benchmarks against which we can evaluate the success of our new design.

The aim is to improve our familiarity with the relevant experimental procedures, whilst learning how to handle microwave electronics and the best practices for conducting a good experiment with microwaves. In addition, we hope to better understand factors (e.g. loss mechanisms) that can affect experimental results.

5.1 Aluminium Cavity

This section will describe the experimental set-up and procedures for characterising the aluminium cavity. Following this, will be a presentation and analysis of the results obtained. We will conclude with a summary of the overall cavity performance; comparison with expected behaviour and lessons that can be drawn from this.

5.1.1 Laboratory Set-Up

The table below provides details on the equipment used in the set-up, including information on manufacturer and model number.

Component	Manufacturer	Model No.	Notes
Signal Generator	Tektronix	AFG2021	-
Microwave Generator	Anritsu	MG3692C	20 GHz
Lock-In Amplifier	Stanford Research Systems	SR830	-
Microwave Diode	Anritsu	75KC50	10 MHz – 40 GHz
Directional Coupler	Marki	C10-0226	-

Table 12: List of equipment used in experiment

Our set-up is shown in the following photograph and schematic diagram.

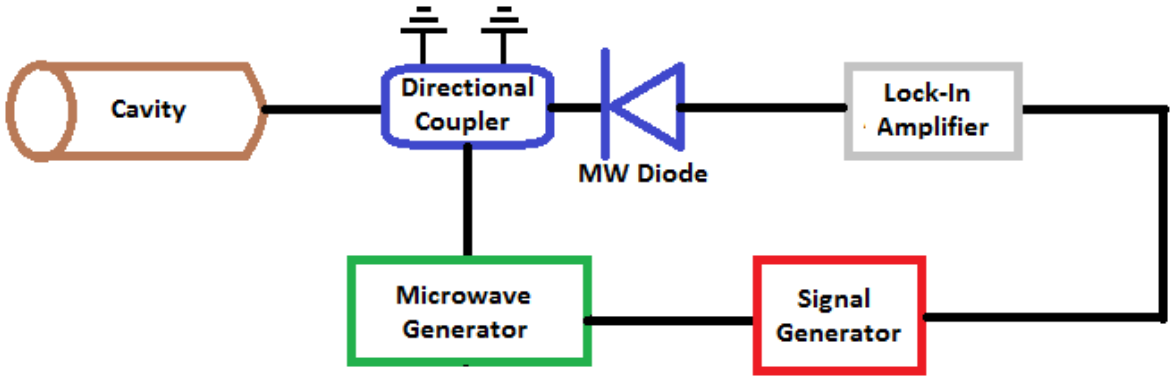

Figure 22: Experimental set-up schematic diagram

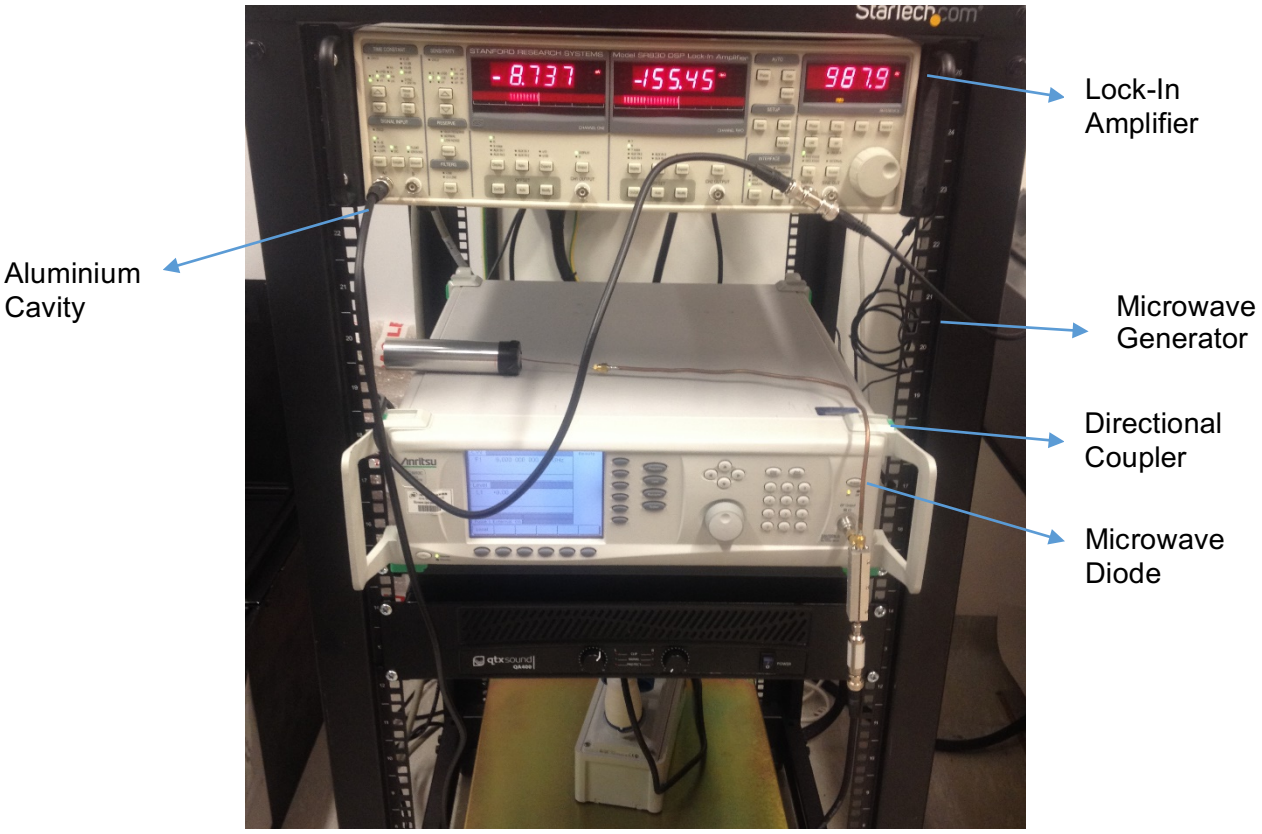

Figure 23: Experimental set-up photograph

It should be noted, that the signal generator, at the top of the rack, is not visible in the above photograph. Below is a brief description of operation for some of the components.

- The **microwave diode** changes power (W) to volts (V)
- The **directional coupler** provides input from the microwave source, as well as referencing it
    - Power goes through the DC, but part of it is kept aside whilst the rest travels through to the cavity
    - Some reflects back and the rest is added to what was originally sectioned
    - This improves the SNR
- The **signal generator** provides the reference signal to the **microwave source** and **lock-in amplifier**, to ensure that they're pulsing energy at the same time

5.1.2 Dimension Measurements

Cavity dimensions were measured using the vernier caliper, pictured below. The following table contains key measurements taken.

Dimension	Value (mm)
Full Length	120
Cavity Length	17
Radius	12.65
Wall Thickness	2.7

Table 13: Dimensions of aluminium cavity

Photographs of the cavity, supplemented by a schematic diagram, are shown below.

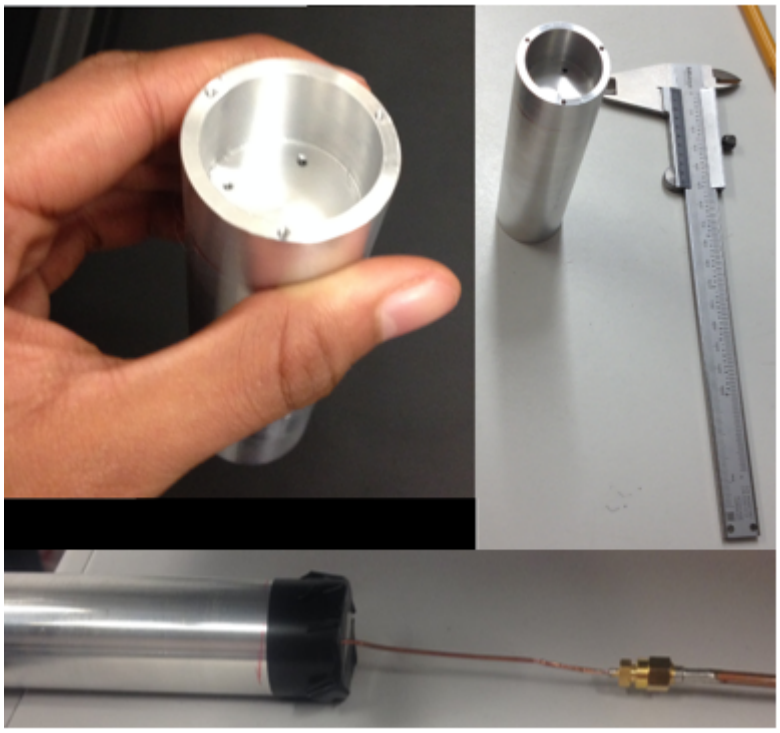

Figure 24: Aluminium cavity photographs

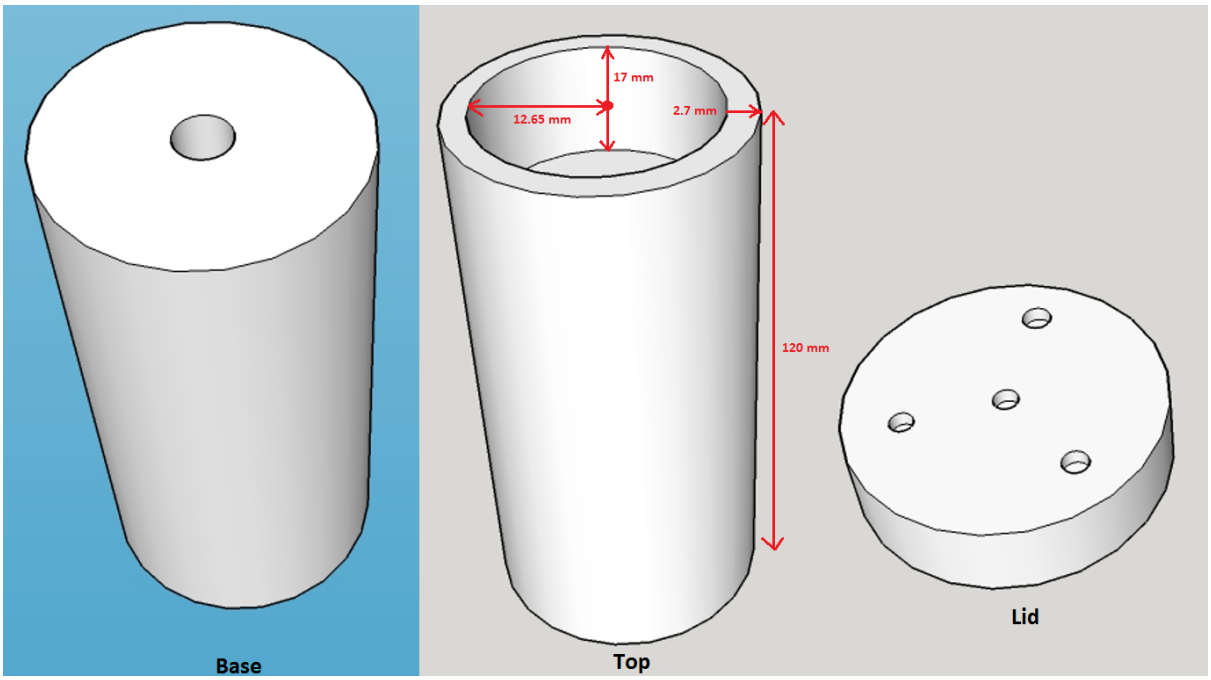

Figure 25: Aluminium cavity schematic diagram

5.1.3 Experimental Procedure

In order to perform the experiment, we completed the following steps:

1. Place the lid on the cavity and secure it with electrical tape
2. Use the tape to cover holes on the lid that are not required (all except for the central one), to prevent the propagation of unwanted modes

3. Insert the coupling wire into the cavity via the central hole on the lid; the wire is connected to a microwave source, which supplies the power
4. Conduct an initial frequency sweep over a broad range (2 – 20 GHz), using a moderate step size (0.01)
5. Once the resonant frequency peak has been identified, gradually narrow the range of subsequent frequency sweeps until it is more pronounced

Upon identifying a peak, it can be verified by changing the coupling to the cavity. By pushing the wire slightly further in, we can worsen the coupling. If the peak has been correctly identified, there will be a visible reduction in its signal strength at the resonant frequency.

The above process helps to distinguish useful observations from anomalies. This is particularly useful in the case of standing waves, which could occur due to poor wire quality. For example, the waves could be reflecting off of a crack in the wire, prior to reaching the end of the cavity. Additionally, the coupling wire has some intrinsic energy losses which manifest as heat. These losses can be compensated by applying more input power.

5.1.4 Results

The frequency sweeps were performed using LabVIEW and the results automatically stored in a text file, with each row corresponding to a different frequency in the format: [frequency (GHz), measured voltage (V)].

Using OriginPro, a data analysis and graphing software, the results were plotted. A curve was then fitted using the Lorentz fit, to enable accurate analysis.

A summary of our results, for each frequency sweep, is displayed in the table below.

f1 (GHz)	f2 (GHz)	∆f	Test No.	xc	w	Q-factor
2	20	0.01	1	15.2	0.841	18.1
5	10	0.01	1	9.22	5.15	1.79
5	10	0.01	2	9.24	1.02	9.06
8	10	0.001	1	8.90	0.0837	106
8.5	9	0.001	1	8.90	0.0297	300

Table 14: Frequency sweep results for Al cavity

The Q-factor was calculated by dividing the resonant frequency (xc) by the FWHM (w).
It can be observed that, as we narrow the frequency window, the results get worse before improving. This was due to a deliberate distortion of the coupling to verify the peak, for the reasons outlined earlier. Furthermore, we can see that as the step size (∆f) reduces, the accuracy improves.

The graph below shows the frequency sweep results in the 2 – 20 GHz range. In this case, the peak is difficult to identify. Moreover, Origin is not able to identify the peak if there are too many data points (i.e. the range is too broad). Therefore, it is important to minimise the range around the peak for accurate results.

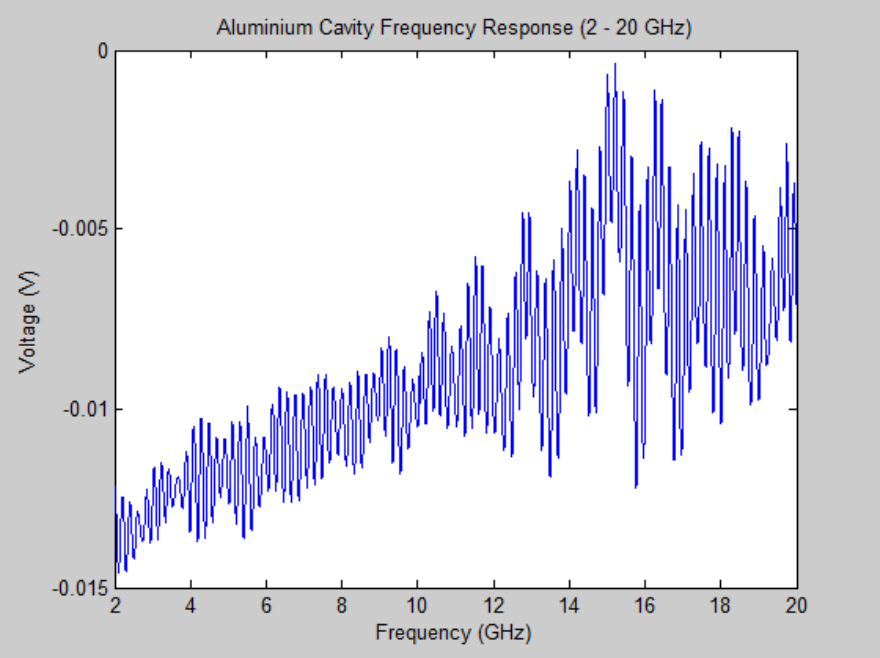

Figure 26: Al cavity response between 2-20 GHz

The next graph displays results within the 5 – 10 GHz range. A peak can be seen more clearly within the vicinity of 9 GHz. However, it is still too broad to generate an accurate Lorentz fitting.

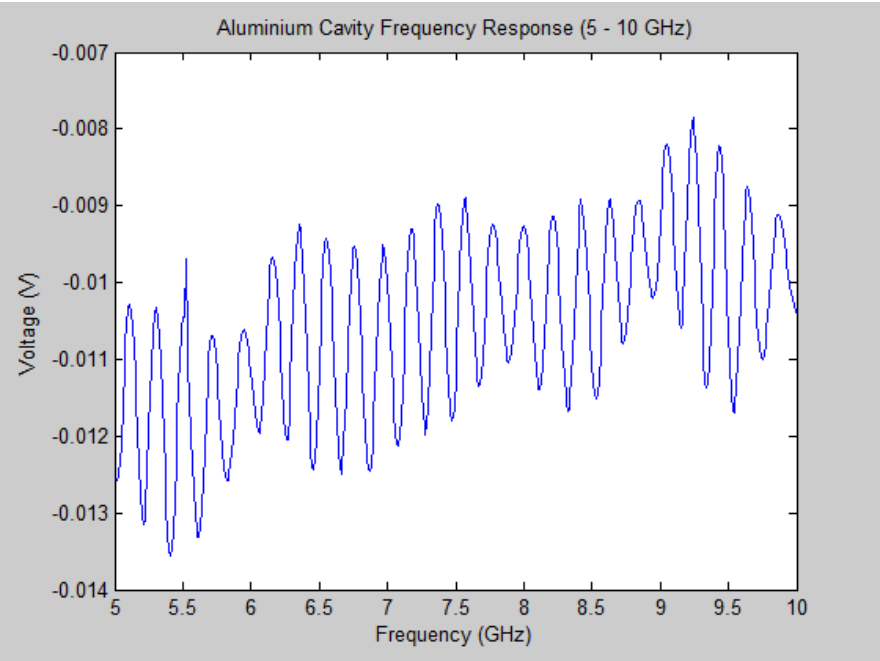

Figure 27: Al cavity response between 5-10 GHz

In our next experiment, we narrowed the frequency range further to 8 – 10 GHz, as well as reducing the step size to 0.001. These results are much better and allow us to perform a Lorentz fitting (red line), which is displayed below.

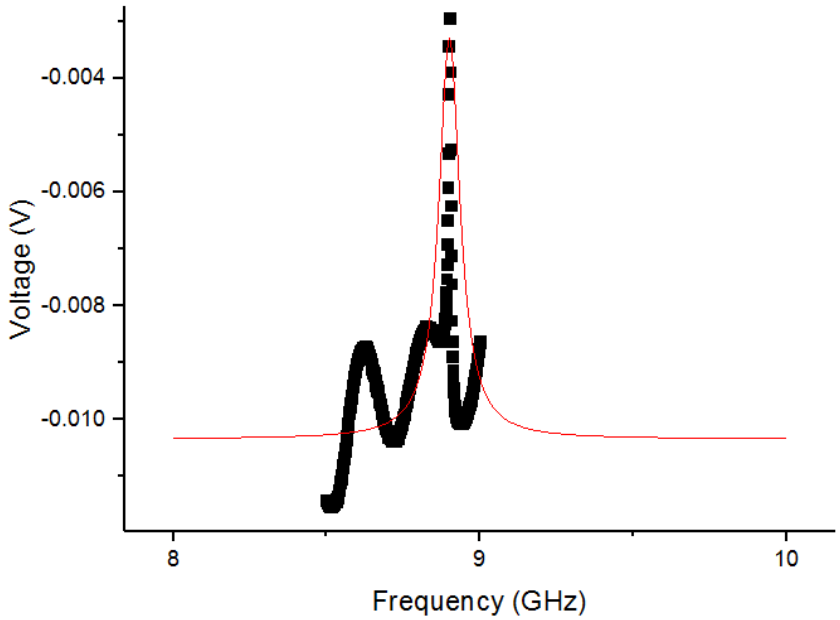

Figure 28: Al cavity response between 8-10 GHz

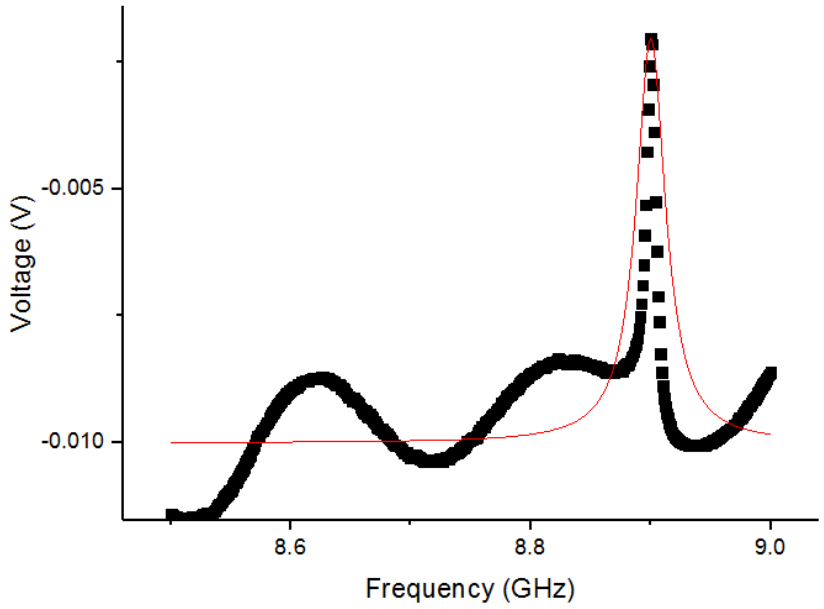

Figure 29: Al cavity response between 8.5-9 GHz

For our final experiment with the aluminium cavity, we closed in on the peak by performing a frequency sweep between 8.5 – 9 GHz and using a step size of 0.001. This yielded a correct value for Q-factor, which was 300.

5.1.5 Excited Modes

Following the measurement of the cavity dimensions, we were able to determine the various modes that would be excited and the corresponding frequencies for these. The graph below, aided in this analysis.

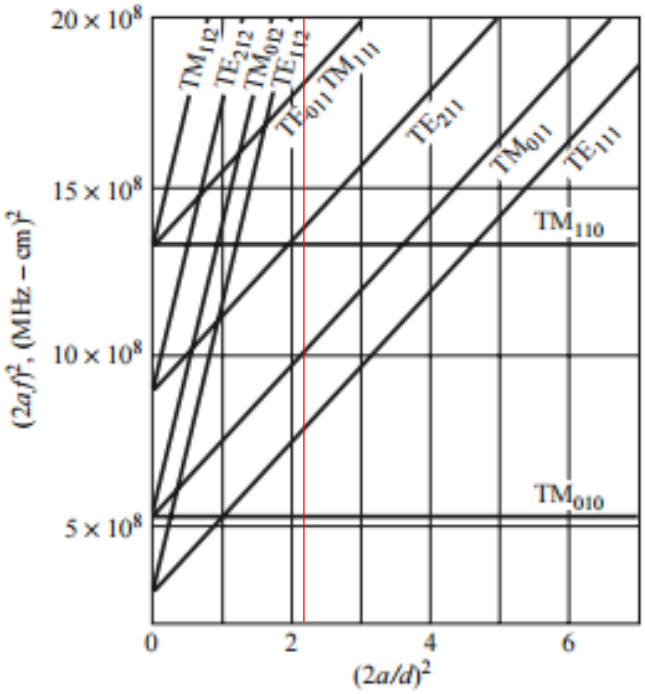

Figure 30: Resonant mode chart for a cylindrical cavity (Pozar)

By calculating the a/d ratio from the measurements, we were able to trace a vertical line (red) across the graph and pinpoint the intersections with various modes.

$$\left(\frac{2a}{d}\right)^2 = \left(\frac{2 \times 12.65}{17}\right)^2 = 2.2$$

The table below displays the excited modes and the frequencies at which each of these occur.

Mode	TM 010	TE 111	TM 011	TM 110	TE 211	TE 011
Frequency (GHz)	9.27	10.8	12.5	14.3	14.7	16.5

Table 15: Excited modes for aluminium cavity

Our detected resonant frequency was around 9 GHz, which corresponds to the TM_{010} mode, as expected.

5.1.6 Summary

From performing these experiments, we were able to determine the Q-factor and resonant frequency of the aluminium microwave cavity. We learnt important details about the required experimental procedure and how it can be used to correctly identify a peak. The final Q-factor of the cavity was measured to be 300, with a resonant frequency of approximately 9 GHz.

5.2 Copper Cavity

This section will provide an analysis and discussion of the copper cavity. The experimental set-up and procedure are identical to that which was described earlier, for the aluminium cavity. Therefore, it will not be repeated. Instead, the focus will be on characterising the cavity through a series of experiments.

5.2.1 Dimension Measurements

The following table contains key measurements.

Dimension	Value (mm)
Full Length	99
Cavity Length	14
Radius	9.5
Wall Thickness	3

Table 16: Dimensions of copper cavity

Photographs of the copper cavity are displayed below.

Figure 31: Copper cavity photographs

5.2.2 Results

In the same way as before, we performed multiple frequency sweeps using the copper cavity. The resulting data was plotted and analysed using MATLAB and OriginPro.
The best result was achieved within the 11 – 13 GHz range and a peak can clearly be seen around 12 GHz.

The Q-factor was calculated as follows:

$$Q = \frac{f_{res}}{FWHM} = \frac{xc}{w} = \frac{12.073}{0.00597} = 2{,}022.3$$

As expected, the Q-factor is approximately 2,000.
The graph below shows the results of our initial frequency sweep between 10 – 20 GHz. A peak can be seen at around 12 GHz.

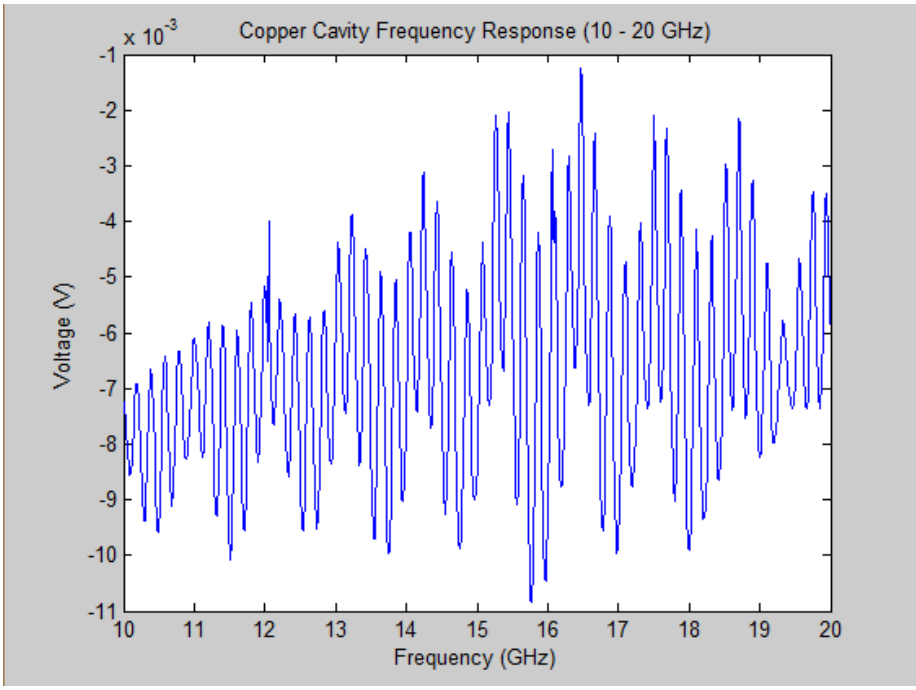

Figure 32: Cu cavity response between 10-20 GHz

In order to verify this, we narrowed our frequency range further to 10-14 GHz and saw that there was resonance in the vicinity of 12 GHz.

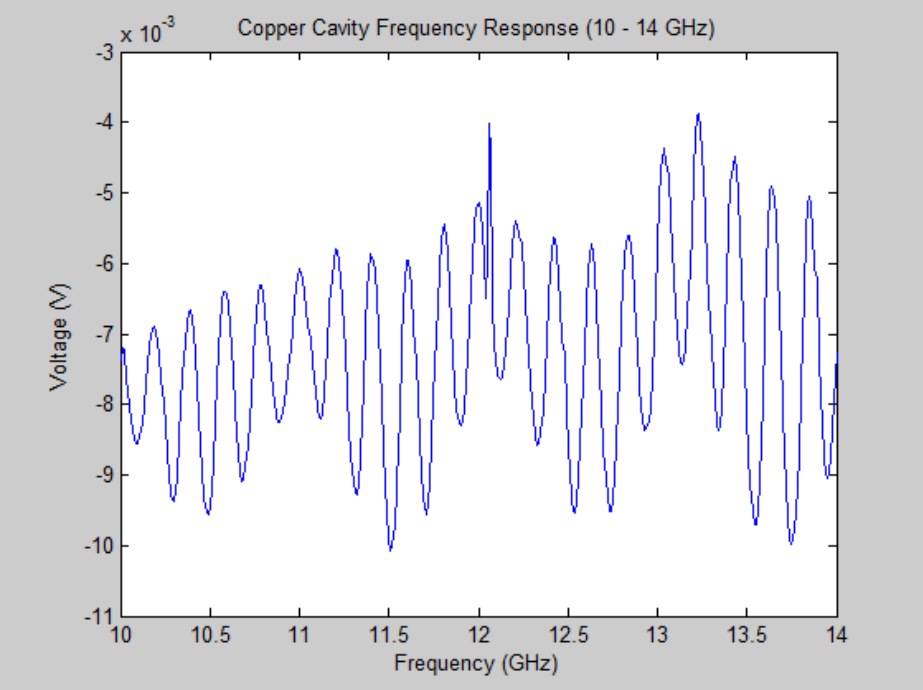

Figure 33: Cu cavity response between 10-14 GHz

As with the aluminium cavity, we deliberately worsened the coupling in between runs to verify the peak. Once we were certain of the peak, we gradually increased the coupling until maximum absorption was achieved. The best result is displayed below.

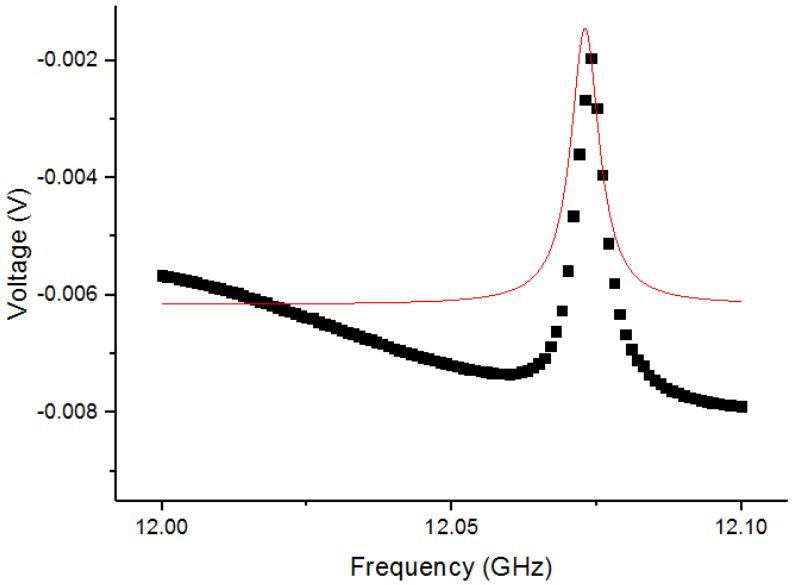

Figure 34: Cu cavity response between 11.5-12.5 GHz

5.2.3 Excited Modes

Using the same procedure as for the aluminium cavity, we determined the modes that will be excited at particular frequencies. The results are displayed in the table below.

Mode	TM 010	TE 111	TM 011	TE 211	TM 110	TE 011	TE 112
Frequency (GHz)	12.3	13.9	16.1	18.8	19	21.7	22.3

Table 17: Excited modes for copper cavity

Again, as expected, the resonant mode for this experiment was TM010. This is clear from the fact that our resonant frequency was approximately 12 GHz.

Overall, the copper cavity was found to have a Q-factor of approximately 2,000 and a resonant frequency of 12 GHz.

5.2.4 Comparison

Overall, the copper cavity displayed superior performance characteristics. This was mostly due to its much higher Q-factor. As mentioned earlier in this report, greater sensitivity and absorption across narrow frequency ranges are among our main goals. For this, the copper cavity is more appropriate.

5.3 Comparison between Cu (Copper) and Al (Aluminium) cavities:

The 2 cavity materials currently used in the lab are Cu (Copper) and Al (Aluminium). Thus, whilst narrowing our design choices we had a choice between these 2 materials. This section aims to compare these 2 materials qualitatively and quantitatively. This section also draws on from the numerical results from the Characterisation Existing Cavities (section 5), in which we performed experiments on both Cu and Al cavities to help us narrow our choices.

5.3.1 Qualitative comparison between Cu and Al:

As mentioned in the Cavity Design (section 3) of our report, we need to ideally design a cavity that achieves the best compromise between the resonant frequency and Q factor. This is above the fact that we also have certain dimensional restrictions we have to adhere to; this

again is mentioned in the Cavity Design (section 3) of our report. Although apart from this we also had other factors to take into account like cost and oxidisation of the cavity material.

Cost: Ideally we would like to choose the material with a lower cost, as this would be beneficial whilst producing the final cavity. In terms of cost Al is cheaper than Cu.

Oxidisation: Ideally our cavity material would not suffer from oxidisation. This is because oxidisation changes the surface resistivity of the cavity and negatively impacts the Q factor, lowering it. In view of this fact, a material like gold would be the ideal material to design the cavity with. Although the cost involved with Gold is unreasonably high. Comparing Copper and Aluminium, both are at the same level where oxidisation is concerned as both oxidise a similar amount in air. Thus, there is negligible difference between these 2 materials. However, Cu does have a slight advantage, as the oxidisation is much more visible on a Cu cavity that Al cavity. Thus, making it easier to spot the oxidisation for Copper allows us to take corrective measures, whilst Al cavity retains its shine making it harder to spot the oxidisation.

5.3.2 Quantitative comparison of Cu and Al Cavities

All the values mentioned in this sub section were obtained from Characterising the Existing Cavities (section 5) in the lab. Thus, refer to the Characterising of Existing Cavities (section 5) for experimental details.

Resonant Frequency: From the Cavity Design (section 3) it was mentioned that we ideally need a resonant frequency between 2-8 GHz. On characterising the existing Cu and Al cavities we found that for the TM010 mode Cu had a resonant frequency of 12 GHz and Al for the TM010 mode had a resonant frequency of 9 GHz. None of the existing cavities had a resonant frequency in our desired target range. However, this was expected, as it was our aim to redesign to obtained resonant frequency within the 2-8GHz ranges. Although Al's resonant frequency was closer to falling within our desired range in comparison to Cu.

Q factor: From the Cavity Design (section 3) it was mentioned that we ideally need a Q factor that was as high as possible (maximise absorption). On characterising the existing Cu and Al cavities we found that Cu had a Q factor of 2000 and Al had a Q factor of 300. Thus, it is seen here that there is a huge difference (1700) between the obtained Q factors for the Cu and Al cavities.

	Copper (Cu)	**Aluminium (Al)**
Cost	More expensive	Cheaper/Less expensive
Oxidisation	Both similar	Both similar
Resonant Frequency	12 GHz	9 GHz
Q factor	2000	300

Table 18:Table summarising the difference between Cu and Al

5.3.3 Final Choice of material:

After considering our design needs and the above factors we made a choice to go with Copper as our desired material of choice. This was mainly because although Copper is more expensive than Aluminium, the Q factor obtained for Copper is much higher than that of Aluminium. Additionally, Cu is not exponentially more expensive than Al and its much bigger Q factor makes up for higher cost. Thus, as one of our main design goals is improving the performance characteristics we believed the much larger Q factor was an important deciding factor. Following this we solely investigated copper as a material and performed all calculations and simulations for a Copper cavity.

6 Cavity Simulations

As mentioned in the Calculations Section (Section 4), we narrowed down our design choice to 3 cavity measurements. We then simulated these cavity designs in CST Microwave Studio. The purpose of these simulations was to cross check our hypothesis about the field patterns (Electric and Magnetic field) in the cavity and confirm our Q factor and resonant frequency figures obtained from the calculations performed. This would then help us narrow down on a final design measurement. Thereby, completing the aim of the project- designing a new cavity with improved resonant frequency and Q factor to perform FMR experiments.

This section will discuss the simulation results obtained for the 3 narrowed down measurements individually. The 3 cavity design measurements we narrowed to simulate are shown in the table below, which is explained in the Cavity Design (Sections 3) of the report.

a (mm)	d (mm)	f (GHz)	Q-factor
14.5	50	7.9	15,300
14.5	29	7.9	13,160
14.5	10	7.9	8,000

Table 19: Table showing our final cavity design dimensions simulated.

6.1 Simulation Design 1 – 14.5mm x 10mm

The below diagrams show the Electric field and Magnetic field diagram patterns obtained for the designed cavity of this dimension. This diagram is for the TM010 mode; this mode has a strong Electric field component in the z direction. The Magnetic field component of this mode is circular and minimal at the centre.

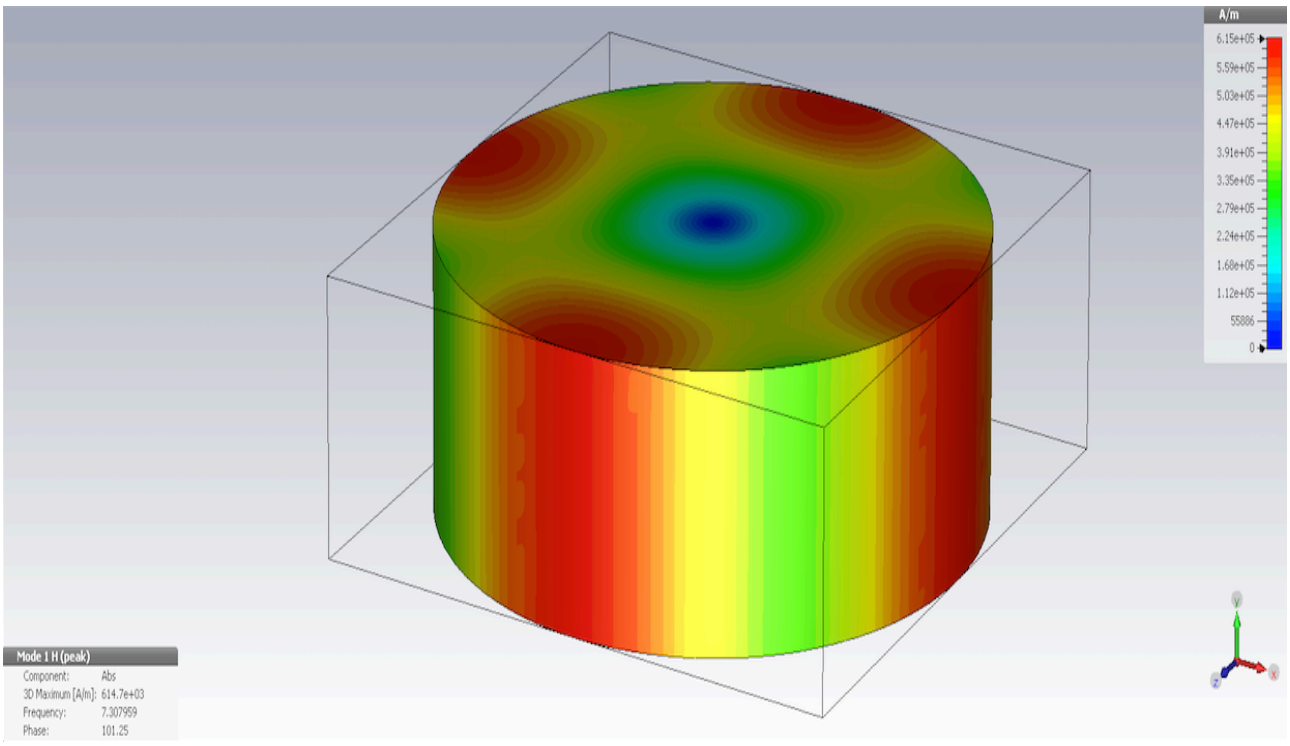

Figure 35: Simulation result of Magnetic field pattern for the above measurement cavity design for TM010 mode

6.1.1 Q factor results obtained for this measurement (14.5mm x 10mm)

14.5mmx10mm	Q factor	Resonant Frequency/GHz
Mode 1 (TM010)	7590.3	7.310
Mode 2	9604.4	11.557
Mode 3	9597.8	11.556
Mode 4	1097.0	14.619

Table 20: Table shows numerical results obtained for the above cavity design measurement for different modes

For this mode comparing the Q factor obtained from the simulations to that obtained in our calculations, 7590 compared to predicted value from calculation of 8000. Thus, this aligns with our prediction, as there is a relatively small difference compared to the calculated value (0.05%). This is also true for the resonant frequency as we predicted (through calculations) a resonant frequency of 7.9GHz for TM010 mode and the simulations gave a resonant frequency of 7.31GHz as seen from above table for this mode.
Further, we also looked at the resonant frequency of other modes for this cavity design measurement. This was done to see if the mode frequencies are close together or far apart, as this affects the ease by which we can distinguish the different modes. For this cavity design as can be seen by the results for the other modes (Modes 2,3 and 4), the resonant frequency falls between 11-14GHz. Thereby, also making the TM010 mode easily distinguishable.

6.2 Simulation Design 2 – 14.5mm x 50mm

The below diagrams show the Electric field and Magnetic field diagram patterns obtained for the designed cavity of this dimension for the TM010 mode. As mentioned, in this mode the Electric field is strong in the z direction, whilst the magnetic field is circular and minimal at the centre.

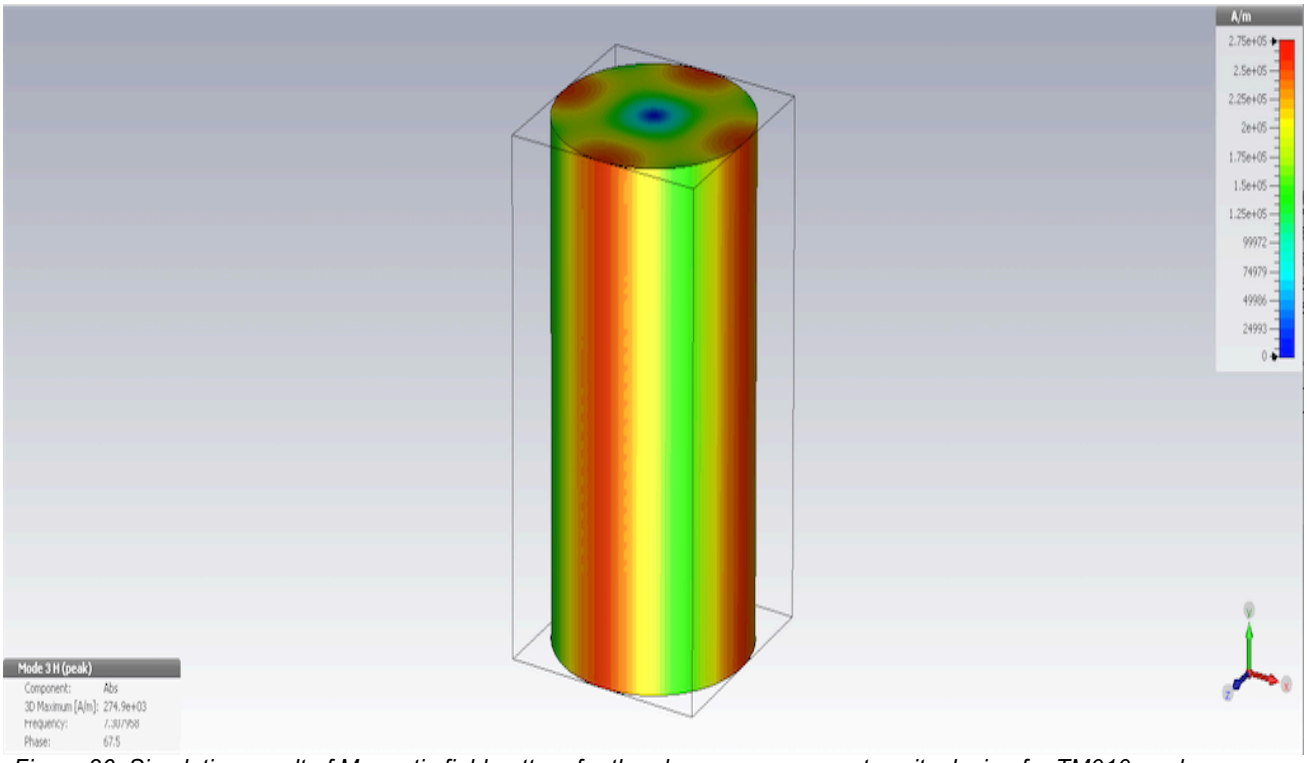

Figure 36: Simulation result of Magnetic field pattern for the above measurement cavity design for TM010 mode

6.2.1 Q factor results obtained for this measurement (14.5mm x 50mm)

14.5mmx50mm	Q factor	Resonant Frequency/GHz
Mode 1	12108	5.975
Mode 2	12111	5.976
Mode 3 (TM010)	14254	7.310
Mode 4	12150	7.900

Table 21: Table shows numerical results obtained for the above cavity design measurement for the different modes

For this mode comparing the Q factor obtained from the simulations to that obtained in our calculations, 14254 compared to predicted value from calculation of 15000. Thus, this again aligns with our prediction, as there is a small difference compared to the calculated value (0.049%). This is also true for the resonant frequency as we predicted (through calculations) a resonant frequency of 7.9GHz for TM010 mode and the simulations gave a resonant frequency of 7.3GHz as seen from above table for this mode.

We again observed the resonant frequencies of the other modes. This again was positive as the two of the other modes fell at a frequency of 6GHz.Thus, making the TM010 mode easily distinguishable from these two modes.

Although 1 mode (mode 4) fell at a frequency of 7.9GHz, which although is close to the TM010 mode's resonant frequency of 7.31GHz, we believe that it offers sufficient space to distinguish the TM010 mode. These results for the other modes are shown in the table above.

6.3 Simulation Design 3 – 14.5mm x 29mm

The below diagrams show the Electric field and Magnetic field diagram patterns obtained for the designed cavity of this dimension for the TM010 mode. The Electric and Magnetic field for the TM010 mode follow the same pattern as described for the above two measurement simulations.

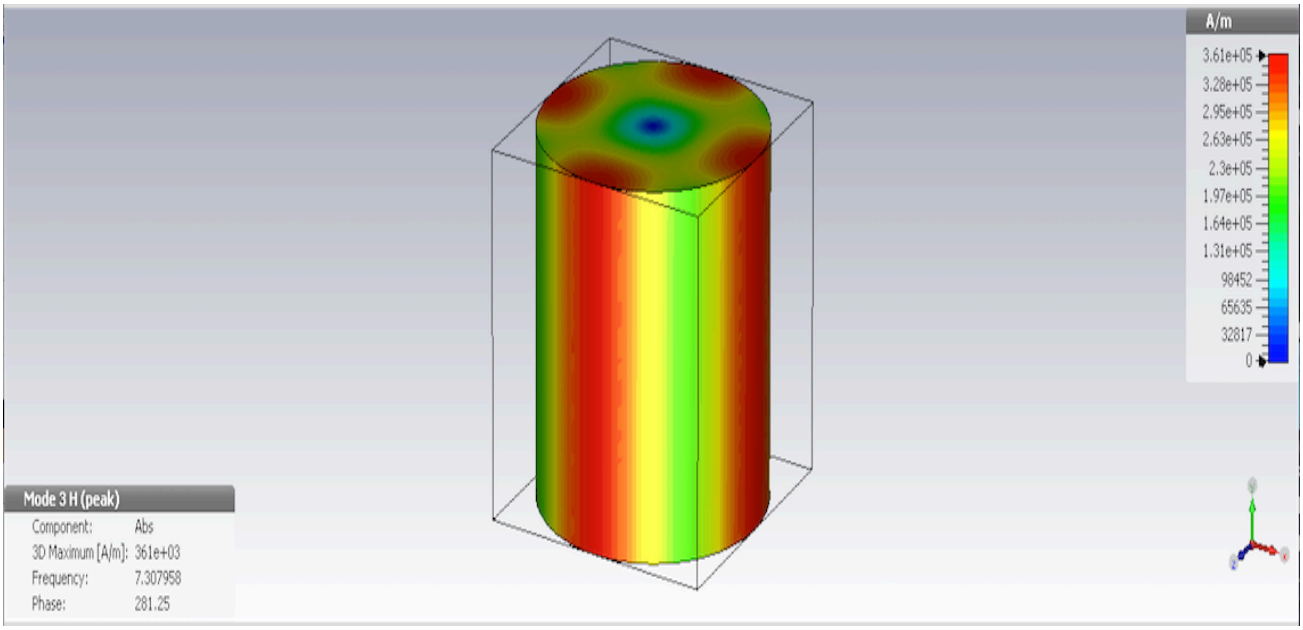

Figure 37: Simulation result of Magnetic field pattern for the above measurement cavity design for the TM010 mode

6.3.1 Q factor results obtained for this measurement (14.5mm x29mm)

14.5mmx29mm	Q factor	Resonant Frequency/GHz
Mode 1	12436	7.308
Mode 2	12439	7.309
Mode 3 (TM010)	12302	7.310
Mode 4	10259.0	8.953

Table 22: Table shows numerical results obtained for the above cavity design measurement for the different modes

The simulation results for this cavity design measurement also align with our predicted calculated values. The simulations for TM010 mode give us a Q factor of 12302 as compared to a calculated value of 13160. Thus a relatively small difference compared to the calculated value (0.065%). Similarly. for the resonant frequency, we calculated a resonant frequency of 7.9GHz, the simulation value of 7.31 as seen in the above table aligned with our calculated value for the TM010

Additionally, we compared the resonant frequency of the TM010 to that for the other modes in this design. We observed for this design the other modes also have a resonant frequencies very close to 7.3GHz. This can be seen in the table above too, which shows the resonant frequency and Q factor results for the other modes. Thus, in this design it may be harder to distinguish between the TM010 mode and other modes by looking at the resonant frequency alone and other methods (like calculating the Q factor, observing the field patterns) will have to be used.

6.4 Conclusion from simulation results

From observing the simulation results we can conclude that our predicted values for the resonant frequency and Q factor align/match the ones obtained from simulations. The maximum variation we got out of the above 3 designs was 0.06% for the 14.5mmx29mm dimension. Thus, showing our original hypothesis and calculation are correct. It is also important to note the Q factors for all dimensions were in the 1000's and the resonant frequency below 8GHz. Thus, also sticking to the improved cavity design requirements that were originally set.

The tables below summarise the difference between obtained and calculated Q factor and resonant frequency values, for the 3 dimensions simulated.

Dimension	Calculated Q factor	Obtained Q factor	Difference
14.5mm x 10mm	8000	7590.3	409.7
14.5mm x 50mm	15300	14254	1046
14.5mm x 29mm	13160	12302	858

Table 23: Table summarising the difference between obtained and calculated Q factors for the 3 dimensions simulated

Dimension	Calculated Resonant Frequency	Obtained Resonant frequency	Difference
14.5mm x 10mm	7.900	7.310	0.59
14.5mm x 50mm	7.900	7.310	0.59
14.5mm x 29mm	7.900	7.310	0.59

Table 24: Table summarising the difference between obtained and calculated resonant frequencies for the 3 dimensions simulated

Further, from observing the Electric and Magnetic field patterns for the TM010 mode for our design in all three dimensions above we observed a strong definition of Electric and magnetic fields that are easily distinguishable from each other (Electric field is negligible when the magnetic field is maximum). This allows us to place the sample in whichever field we choose to and know where mainly in the cavity which field will exist.

Lastly, apart from the 14.5mm x 29mm the resonant frequency of the other modes were easily distinguishable from that of the TM010 mode (9.3GHz). Thus allowing us to easily identify the TM010 mode. Therefore, in conclusion we believe that the simulations have confirmed our original calculations and hypothesis.

Thus to conclude, all the above designs we simulated satisfied the 3 main criteria we set out at the start – High Q factor, low resonant frequency between 2-8GHz and strong electric and magnetic fields that can be distinguished easily. However, for our final design choice we decided to send the 14.5mm x 29mm cavity dimension measurement for production. This is because it had a much higher Q factor as compared to the 10mm length and although it's Q factor was slightly lower than the 50mm length, we believed that a length of 29mm would be more compatible with the existing equipment/machinery in the lab.

7 Conclusion

7.1 Summary of Goals & Objectives

The ultimate aim of this project, was to design an optimal microwave to provide accurate detections of spin dynamics in thin-film samples. In order to achieve this, we decided to focus on a few key characteristics that would result in an ultra-sensitive cavity. These were:

- High Q-factor, in the thousands, for absorption across a narrow frequency range
- Low resonant frequency, ideally between 2 – 8 GHz, for practical reasons as well as better noise performance
- Strong electric and magnetic fields, which do not overlap and are easily distinguishable from each other

We also had to ensure that the design adhered to any constraints imposed by cost of materials or restrictions in manufacturing capabilities.

7.2 Design Methodology

We began by conducting extensive research into microwave cavities and the parameters that affect their performance characteristics. By collating information from various sources and literature pertaining to microwave engineering, we determined the equations needed to form the basis of our subsequent computations.
For each dielectric material (air, FR4, PTFE), we conducted a separate set of calculations. Most of the parameters remained constant in each set, so our only variables were dimensions.

Thus, we examined the effect of altering the radius or length of our cavity on the Q-factor and resonant frequency.
Air turned out to be the superior dielectric, so we narrowed down our design to three sets of dimensions for simulation. We then examined the simulation results to see how closely they matched our hypothesis and which design displayed the best performance characteristics.

7.3 Final Design

When deciding on the properties of our final design, we took into consideration: material, shape, resonant mode, dielectric material and dimensions. Details of the decision making process are outlined in the earlier sections of the report. Below is a summary.

Parameter	Value
Material	Copper (Cu)
Shape	Cylinder
Resonant Mode	TM_{010}
Dielectric	Air
Cavity Length (mm)	29
Radius (mm)	14.5
Wall Thickness (mm)	3
Predicted Q-factor	13,160
Predicted Resonant Frequency (GHz)	7.9

Table 25: Final cavity properties

Below is a 3D diagram of the cavity that was submitted for production, with the stated specifications.

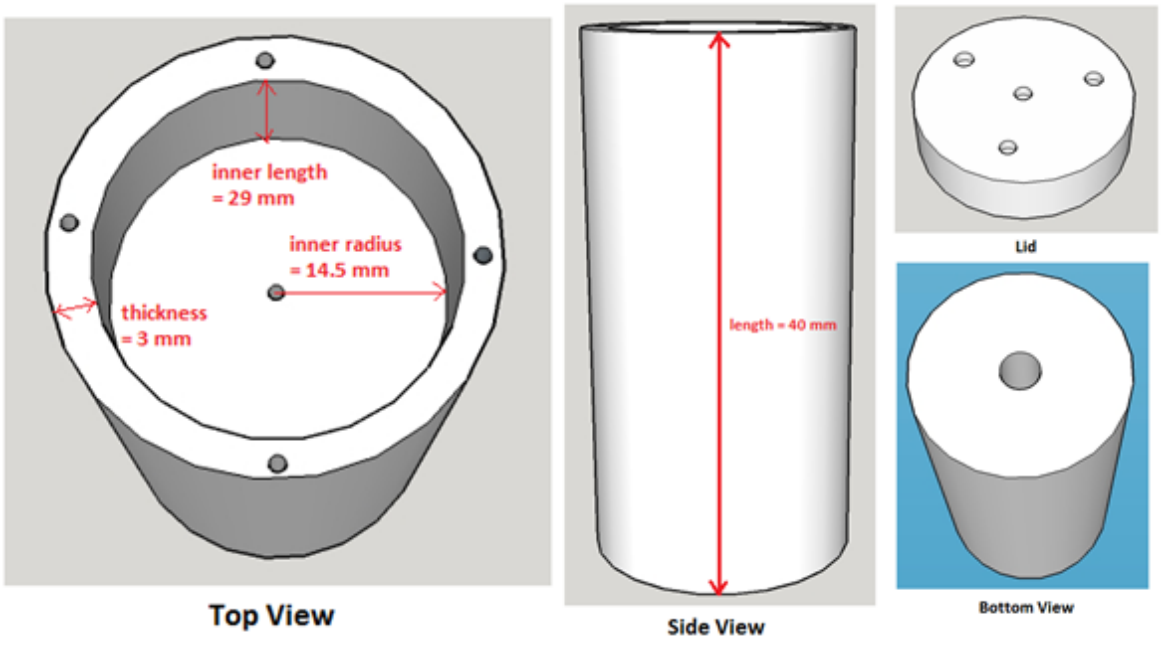

Figure 38: Final design 3D model

7.4 Characterising Existing Cavities

We characterised two existing cavities in a laboratory environment to test which material gives a better result. Ultimately, we found copper to be a better material. Although it had a slightly higher resonant frequency, the Q-factor was almost sevenfold higher than aluminium and more than compensated for this.

7.5 Simulation Results

The simulation results verified our initial hypothesis. The resulting Q-factors and resonant frequencies aligned with our predictions, with relatively little error, for each set of dimensions submitted. As expected, the resonant frequency remained roughly the same due to the radius being kept constant. Additionally, the simulations confirmed that an increased length results in a higher Q-factor.

The field diagrams generated, also showed that the electric and magnetic fields can be easily identified without any overlap. Furthermore, as we expected, no two modes are excited at the same frequency.

7.6 Summary

To conclude, we undertook a number of steps in designing an ultra-sensitive microwave cavity. To this effect, we selected materials (Cu) and a dielectric (air) with a high Q-factor, as well as dimensions that kept us within the target resonant frequency range. The simulations showed easily distinguishable field lines, which do not overlap, and confirmed our hypothesis. Overall, we were successful in designing an optical cavity and achieved our initial goals.

8 Reflection

8.1 Production Delays

One of the main deliverables of this project post the research and design was an upgraded microwave cavity to provide accurate spin detections. Unfortunately, there has been a significant delay in the production of this cavity. For this reason, we are not able to conduct any experiments on it to measure its performance and validate our hypothesis.

We expected the experiments conducted on the final cavity and its performance analysis to constitute a substantial part of our report. However, due to factors beyond our control, this is no longer possible. As a result, the report will not have as many experimental results or analyses as expected.

The team had completed all required testing and calculations much earlier than predicted and submitted the final design well in time to carry out the aforementioned tasks. It was communicated to us that cavity production would take less than a week. Despite this, we submitted our design well in advance to avoid any unexpected issues. Unfortunately, it was still not produced in time for us to perform the required experiments. We had hoped to carry out experiments beyond the original project scope by ensuring all efforts from our side were completed well in advance; this would have not only added value to our knowledge, but would have also helped further the research and allow us to make a worthwhile contribution to this field.

8.2 Contingency planning

The work plans also had to be altered and division of tasks as stated in the project proposal was no longer valid. Having landed in such an unfortunate situation, we devised a contingency plan in order to still enhance the quality of the report, as well as enrich our practical understanding of the theoretical concepts that would have been covered while experimenting with the final cavity: We requested additional lab sessions to perform further experiments on the existing microwave cavities. Unfortunately, this could not be arranged for us. And as we require supervision to access the labs in LCN and perform these experiments, it was beyond our control to do anything more.

9 Further work

9.1 Experiments we would perform if we had more time

The new cavity will need to go through the same experiments that were conducted for the Copper and Aluminium cavities. While the frequency is being swept within the range we calculated the resonant frequency to occur in, peaks need to observed. Once the accurate resonant frequency is determined, the mode under which the cavity is operating will need to be found. The main idea is to tune the cavity to achieve the best coupling. We will need to compare the results to the existing cavities and establish if the upgrade was successful in yielding the desired resonant frequency and a high Q-factor. Additionally, the experimental results will need to be compared against the simulation results to observe the similarities and differences and devise a discussion.

9.1.1 FMR and E-field induced FMR

As discussed in the introduction section, FMR is a method used to measure magnetic properties of a ferromagnetic sample by detecting the precessional motion of the magnetisation. (Physik.fu-berlin.de) This phenomenon occurs in materials where all the electron spins point in the same direction in the valence orbital.

There is an existent practical method to measure the ferromagnetic resonance of a sample which could have been used in the lab to test with the new cavity. This would involve a given sample being placed in Ultra High Vacuum (UHV) inside a quartz glass tube, which would consequently fit inside our cylindrical cavity. Beyond this, there would be a magnet. The fact that the magnet and the microwave parts are outside the glass tube makes it very convenient. Other components to be used in this experiment would be similar to other experiments conducted on the existing cavities, including a microwave source, and a detector diode. (Physik.fu-berlin.de)

During this experiment, what we are looking to observe and measure is the absorption derivative/ absorption intensity of the microwaves while the magnetic field is swept.
To take this a step further, after completing FMR experiments on the new cavity, we would have liked to conduct the same on the existing Copper and Aluminium cavities. This would have enabled a wholesome comparison between the old and new cavities beyond that expected within the aims of the project.

A conventional FMR setup is shown in the diagram below.

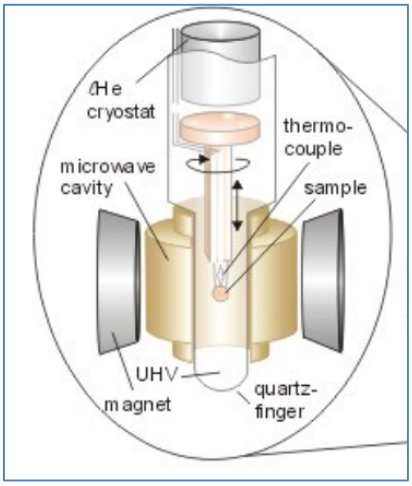

Figure 39: Lab set-up of a typical FMR experiment (Physik.fu-berlin.de)

Conducting experiments to determine the Electric-field-induced Ferromagnetic Resonance was the final task of this project. As it is still a new area being explored within the field, it is difficult to find papers with existing experimental results and analysis for E-field induced ferromagnetic resonance within a microwave cavity resonator like such.

We would ideally like to be able to conduct the aforementioned experiments on the new cavity before the project presentation. Since it is an unexplored area, if we are able to conduct experiments and produce sincere results and analyses, it would be a good step forward and will only have positive influence on furthering the research.

9.2 Contribution to field of spintronics

This research will benefit the field of spintronics by providing more sensitive detections of spin dynamics. The development of microwave cavities as such will allow one to measure thin-film samples, at the same time improving the accuracy of measurements, also.

10 References:

[1] Nave, R. “Ferromagnetism”. [ONLINE] Available at: http://hyperphysics.phy-astr.gsu.edu/hbase/solids/ferro.html [Accessed 29 September 2016].

[2] Nozaki, T.; Shiota, Y.; Miwa, S.; Murakami, S.; Bonell, F.;. Ishibashi, S.; Kubota, H.; Yakushiji, K.; Saruya, T.; Fukushima, A.; Yuasa, S.; Shinjo, T.; Suzuki, Y. “Basic concepts of electric-field-induced FMR in a magnetic tunnel junction with an ultrathin ferromagnetic layer.” Nature Physics (2012). Web. 29 Sept. 2016

[3] “Introduction to Spintronics”. [ONLINE] Available at: http://www.physics.umd.edu/rgroups/spin/intro.html [Accessed 29 September 2016].

[4] Nave, R. Electron Spin. [ONLINE] Available at: http://hyperphysics.phy-astr.gsu.edu/hbase/spin.html. [Accessed 27 September 2016].

[5] “Spin Dynamics”. [ONLINE] Available at: http://physics.bu.edu/~redner/896/spin.pdf [Accessed 29 September 2016].

[6] Merzbacher, Eugen (1998). Quantum Mechanics (3rd ed.). pp. 372ñ3.

[7] Griffiths, David (2005). Introduction to Quantum Mechanics (2nd ed.). pp. 183ñ4.

[8] Wolf, S. A.; Chtchelkanova, A. Y.; Treger, D. M. (2006). "Spintronics: A retrospective and perspective". IBM Journal of Research and Development. 50: 101.

[9] Wolf, S. A. "Spintronics: A Spin-Based Electronics Vision For The Future". Science 294.5546 (2001). Web. 27 Sept. 2016.

[10] Kuch, W. “Ferromagnetic Resonance (FMR)”. [ONLINE] Available at: http://www.physik.fu-berlin.de/einrichtungen/ag/ag-kuch/research/techniques/fmr/index.html [Accessed 20 April 2017]

[11] “Resonant Cavities and Waveguides”. MIT. Available at: http://web.mit.edu/22.09/ClassHandouts/Charged%20Particle%20Accel/CHAP12.PDF. Web. 2 Dec. 2016.

[12] Nassiri, A., “RF Cavities and Components for Resonators”. MIT, USPAS. 2010. Available at: http://uspas.fnal.gov/materials/10MIT/Lecture12.pdf. Web. 2 Dec. 2016

[13] Dr. Kwok, R. “Microwave Engineering”. San Jose State University. Available at: http://www.engr.sjsu.edu/rkwok/EE172/Cavity_Resonator.pdf. Web. 2 Dec. 2016

[14] Pozar, David M. Microwave Engineering. 1st ed. Hoboken, N.J.: Wiley, 2012. Print.

[15] "Microwaves101 | FR-4". Available at: Microwaves101.com. 2017. Web. 23 Jan. 2017.

[16] Li, X. Jiang, Y. "Design of a Cylindrical Cavity Resonator for Measurements of Electrical Properties of Dielectric Materials". 2001. Available at: http://www.divaportal.org/smash/get/diva2:354559/fulltext01. Web. 22 Nov. 2016.

[17] "FR-4 VS. TEFLON PTFE/FEP MACHINING" [ONLINE] Available at: http://www.vanderveerplastics.com/compare-materials.html?sel1=fr-4&sel2=teflon-ptfe-fep. [Accessed 1 Dec. 2016]

[18] Pozar, D. M. "Microwave Engineering", 4th ed. 2012. Available at: http://www2.electron.frba.utn.edu.ar/~jcecconi/Bibliografia/Ocultos/Libros/Microwave_Engineering_David_M_Pozar_4ed_Wiley_2012.pdf. Web. 1 Dec. 2016

[19] Wu, M. W, J. H Jiang, and M. Q Weng. Spin Dynamics In Semiconductors. Amsterdam [u.a.]: Elsevier, 2010. Print.

[20] "Contribution to the Theory of Ferromagnetism". [ONLINE] Available at: http://www.hs-augsburg.de/~harsch/anglica/Chronology/20thC/Ising/isi_fm00.html. [Accessed 28 September 2016].

[21] "Condensed Matter Physics:Spintronics". [ONLINE] Available at: http://www.stoner.leeds.ac.uk/Research/Spintronics [Accessed 29 September 2016].

[22] H. Smith, Carl. "Commercial Applications of Spintronics Technology". [ONLINE] Available at: http://www.nve.com/Downloads/Nanotech2004Spintronics.pdf [Accessed 29 September 2016].

[23] "FR406N DATASHEET". [ONLINE] 2012. Available at: http://www.sbcinc.com/downloads/UL-materials/FR406N.pdf. [Accessed 10 February 2017].

[24] "Teflon PTFE". [ONLINE] Available at: http://www.rjchase.com/ptfe_handbook.pdf. [Accessed 11 February 2017]

11 Appendices:

A. Table showing the effect of altering length (d) on Q-factor and resonant frequency:

a (mm)	d (mm)	a/d	F_{nml} (GHz)	Q-factor
14.5	50	0.29	7.92	15300.92
14.5	29	0.5	7.92	13158.79
14.5	25	0.58	7.92	12492.52
14.5	20	0.725	7.92	11442.42
14.5	15	0.967	7.92	10036.36
14.5	10	1.45	7.92	8056.40

B. Resonant frequencies in the TM_{010} mode, with varying radius (a) for an air dielectric:

a (mm)	d (mm)	a/d	F_{nml} (Hz)
6	12	0.5	19,133,271,042.60
6.2	12.4	0.5	18,516,068,750.91
6.4	12.8	0.5	17,937,441,602.44
6.6	13.2	0.5	17,393,882,766.00
6.8	13.6	0.5	16,882,297,978.77
7.0	14.0	0.5	16,399,946,607.95
7.2	14.4	0.5	15,944,392,535.50
7.4	14.8	0.5	15,513,463,007.52
7.6	15.2	0.5	15,105,213,981.00
7.8	15.6	0.5	14,717,900,802.00
8.0	16.0	0.5	14,349,953,281.95

C. Resonant frequencies in the TM_{011} mode, with varying radius (a) for an air dielectric:

a (mm)	d (mm)	a/d	F_{nml} (Hz)
6	12	0.5	22,849,295,832.21
6.2	12.4	0.5	8,577,402,155,537.16
6.4	12.8	0.5	8,049,690,890,108.61
6.6	13.2	0.5	7,569,222,655,161.82
6.8	13.6	0.5	7,130,522,034,144.65
7.0	14.0	0.5	6,728,884,466,507.12
7.2	14.4	0.5	6,360,249,592,184.58
7.4	14.8	0.5	6,021,098,226,056.41

7.6	15.2	0.5	5,708,368,055,035.47
7.8	15.6	0.5	5,419,384,267,896.92
8.0	16.0	0.5	5,151,802,169,669.51

D. Resonant frequencies in the TM_{111} mode, with varying radius (a) for an air dielectric:

a (mm)	d (mm)	a/d	F_{nml} (Hz)
6	12	0.5	32,945,424,924.41
6.2	12.4	0.5	12,367,390,261,685.80
6.4	12.8	0.5	11,606,505,899,882.80
6.6	13.2	0.5	10,913,739,248,374.70
6.8	13.6	0.5	10,281,195,537,612.50
7.0	14.0	0.5	9,702,091,462,432.68
7.2	14.4	0.5	9,170,572,562,870.40
7.4	14.8	0.5	8,681,564,676,026.32
7.6	15.2	0.5	8,230,652,383,296.42
7.8	15.6	0.5	7,813,978,988,481.29
8.0	16.0	0.5	7,428,163,775,925.02